

New Results on Vacuum Fluctuations: Accelerated Detector versus Inertial Detector in a Quantum Field

I-Chin Wang¹

¹*Institute of Physics, Academia Sinica, Taipei 11529, Taiwan*

We investigate the interaction between a moving detector and a quantum field, especially about how the trajectory of the detector would affect the vacuum fluctuations when the detector is moving in a quantum field (Unruh effect). We focus on two moving detectors system for the future application in quantum teleportation. We find that the trajectory of an uniformly accelerated detector in Rindler space can't be extended to the trajectory that a detector moves at constant velocity. Based on the past work, we redo the calculations and find that a term is missing in the past calculations, also we find that there are some restrictions on the values for the parameters in the solutions. Besides, without including the missing term, the variance from the quantum field for the inertial detector will be zero and is unlikely for such system. Combining all these points, there is a difference on the two-point correlation function between the inertial detector and accelerated detector in early-time region. The influence from proper acceleration can be seen in the two-point correlation functions. This might play a role in the quantum teleportation process and worth to study thoroughly.

PACS numbers: 04.62.+v, 11.27.+d, 98.80.Cq

I. INTRODUCTION

Unruh effect was originally proposed for the studying of Hawking radiation near black hole [1], and it was found that an uniformly accelerated detector would experience a thermal bath at temperature $T_U = \frac{\hbar a}{2\pi c k_B}$, where a is the proper acceleration. It involves the interaction between the background quantum field and a moving detector which has constant acceleration. It is also known that the accelerating charges emit radiation. In the literature [2–9], many physicists were interested in the issue that were there any differences between Unruh effect and the radiation from accelerated charges in the quantum field, for example was the emitted radiation part of the energy flux in the Unruh effect? Later, these issue were extended to the atom system that whether an accelerated atom emitted radiated energy? What was the connection with Unruh effect? Hu and his collaborators worked on the minimal coupling model [10–13] and considered how equilibrium condition and nonequilibrium condition played the role in the accelerated detector [10, 11, 13, 15]. In recent years, this kind of influences between the moving detector and a background quantum filed are applied to some quantum teleportation processes. However, the difference between an inertial trajectory and the uniformly accelerated trajectory for a moving detector is not obvious enough. If we can see the effect about proper acceleration clearly, it would be helpful to the understanding of some important systems, for examples the atomic optical system or a particle quantum filed systems.

Based on the work of Raval, Hu, Anglin, Koks, Johnson and Lin [10–15], here we follow the work of Lin, Chou and Hu [21, 23, 24], and we recheck the computation of uniformly accelerated detector [21](UAD). The solution of UAD [21] was originally supposed that it could be applied to the inertial detector case directly by taking the limit that proper acceleration $a \rightarrow 0$ (i.e. an inertial detector moves at a constant velocity and therefore has a zero proper acceleration). However, when we check the past result about the two-point correlation functions for UAD, we find that the past solution can not be applied to the inertial detector case by taking the limit $a \rightarrow 0$. For an inertial detector moves at constant velocity, we need to apply a real inertial trajectory. In fact, the original goal for our work was applying the past results [21, 23] in some quantum teleportation processes, but some errors occurred when we did it so we have to recheck our set up and calculations. Therefore, we start from the beginning that we apply a real inertial trajectory and the other uniformly accelerating trajectory for the moving detector, solving the solutions for these two trajectories and then comparing the difference on the two-point correlation functions between the inertial and uniformly accelerated detectors.

We find that a term is missing in the past two-point correlation functions and is about the vacuum fluctuations of the moving detector. Without this term, we will have a zero variance from the quantum field for the inertial detector. This part was not noticed before. When we include this term, the strange zero variance issue disappears and the values of the two-point correlation functions also change. This change makes the difference between the inertial and accelerated detector more clear than in the past results. Since we apply perturbations to solve the equations, the

assumptions of perturbation method also set an allowed region for the values of the parameters in the solutions. This restriction also affects the solutions for the two-point correlation functions. Including these considerations, the difference between the inertial detector and accelerated detector is more obvious than ever.

In order to apply our present result in the future work about Quantum teleportation, we consider two moving Unruh-DeWitt detectors in our present model [23]— that are Alice and Bob. We assume that Alice is static in space and Bob is moving in space. Bob’s worldline has two different choices that one is the trajectory for a uniformly acceleration, the other trajectory is for a constant velocity motion. For simplicity, here we focus on the moving detector Bob only and study the interaction between the quantum field and the internal degree of freedom Q for detector Bob, and compute the two-point functions $\langle QQ \rangle_v$ and $\langle \dot{Q}\dot{Q} \rangle_v$ for these two different trajectories(i.e. $\langle QQ \rangle_v$ is the two-point function about vacuum fluctuations of the internal degrees of freedom for Bob), and then we compare the plots of $\langle QQ \rangle_v$ and $\langle \dot{Q}\dot{Q} \rangle_v$ for the inertial and the uniformly accelerating trajectories. We find that these two different types of trajectories have different behavior on the curves for the two-point functions $\langle QQ \rangle_v$ and $\langle \dot{Q}\dot{Q} \rangle_v$ in the early time region. Meanwhile, we also write down a detailed calculations and point out some key points in the calculations for obtaining $\langle QQ \rangle_v$ and $\langle \dot{Q}\dot{Q} \rangle_v$.

To demonstrate the importance of the allowed region on the values of the parameters in this model, we choose some improper values for the parameters in this model and calculate the two-point correlation functions. The improper values would give us a different trend of the two-point functions $\langle QQ \rangle_v$ and make the Unruh effect unclear.

This paper is organized as follows. In Sec. II we set up the model, and introduce the method. In Sec. III we investigate the moving detector Bob in a quantum field and moves at a constant acceleration or at a constant velocity. We solve the solutions for two different trajectories for detector Bob and compute the two-point correlation functions. Then, we discuss the allowed values for the parameters in the solutions and do the numerical plots for the two-point functions. Later, we compare the plots and find out the difference between the inertial detector and accelerated detector. Sec. IV is the summary.

II. MODEL

We consider two Unruh-DeWitt detectors Alice and Bob that are in different spatial point and are in different status of motion. Each detector has the internal degree of freedom Q that interacts with a common scalar field Φ . Assuming that Alice is static and Bob is moving (Bob could be uniformly accelerated or moves at constant velocity, we will calculate the solutions for these two cases later). The trajectories for Alice and Bob are $z_A^\mu(t)$ and $z_B^\mu(\tau)$ respectively. The action for this set up is the following

$$S = - \int d^4x \sqrt{-g} \frac{1}{2} \partial_\mu \Phi(x) \partial^\mu \Phi(x) + \int d\tau_A \frac{m_0}{2} [(\partial_A Q_A)^2 - \Omega_0^2 Q_A^2] + \int d\tau_B \frac{m_0}{2} [(\partial_B Q_B)^2 - \Omega_0^2 Q_B^2] + \lambda_0 \int d^4x \int dt Q_A(t) \Phi(x) \delta^4(x^\mu - z_A^\mu(t)) + \lambda_0 \int d^4x \int d\tau Q_B(\tau) \Phi(x) \delta^4(x^\mu - z_B^\mu(\tau)), \quad (1)$$

where Q_A and Q_B are the internal degrees of freedom for the detector Alice and Bob, they are assumed to be two identical harmonic oscillators with mass $m_0 = 1$ with the bare natural frequency Ω_0 [23].

Suppose that the coupling between the detectors and the field is turned on at when $t = \tau = 0$ (t is the proper time for Alice and τ is the proper time for Bob), the state of this combined system is a direct product of a quantum state $|q_A, q_B\rangle$ for Alice and Bob’s detectors Q_A and Q_B and Minkowski vacuum $|0_M\rangle$ for the field Φ ,

$$|\psi(0)\rangle = |q_A, q_B\rangle \otimes |0_M\rangle, \quad (2)$$

here $|q_A, q_B\rangle$ is taken to be a squeezed Gaussian state with minimal uncertainty, represented in the Wigner function as

$$\begin{aligned} \rho(Q_A, P_A, Q_B, P_B) = & \exp -\frac{1}{8} \left[\frac{\beta^2}{\hbar^2} (Q_A + Q_B)^2 + \frac{1}{\alpha^2} (Q_A - Q_B)^2 \right. \\ & \left. + \frac{\alpha^2}{\hbar^2} (P_A - P_B)^2 + \frac{1}{\beta^2} (P_A + P_B)^2 \right], \end{aligned} \quad (3)$$

which Q_A and Q_B can be entangled by properly choosing the parameters α and β .

Then we quantize the field Φ and the harmonic oscillators Q_A, Q_B in Heisenberg picture, the conjugate momentum $(P(\tau), \Pi(x))$ of these canonical coordinate and momentum $(Q(\tau), \Phi(x))$ are

$$P_d(\tau) = \frac{\delta S}{\delta \dot{Q}_d(\tau)} = \dot{Q}_d(\tau), d = A, B; \quad (4)$$

$$\Pi(\tau) = \frac{\delta S}{\delta \partial_t \Phi(x)} = \partial_t \Phi(x). \quad (5)$$

The equal time commutation relations of these dynamical variables are

$$[\hat{Q}_d(\tau), \hat{P}_d(\tau)] = i\hbar, d = A, B; \quad (6)$$

$$[\hat{\Phi}(t, \mathbf{x}), \hat{\Pi}(t, \mathbf{x}')] = i\hbar \delta^3(\mathbf{x} - \mathbf{x}'). \quad (7)$$

According to the Heisenberg equations of motion, one can write down the equation of motions for \hat{Q} and $\hat{\Phi}$

$$\partial_t^2 \hat{Q}_d(\tau) + \Omega_0^2 \hat{Q}_d(\tau) = \lambda_0 \hat{\Phi}_d(\tau, \mathbf{z}(\tau)), d = A, B; \quad (8)$$

$$(\partial_t^2 - \nabla^2) \hat{\Phi}_d(x) = \lambda_0 \int_0^\infty d\tau \hat{Q}_d(\tau) \delta^4(x - z(\tau)). \quad (9)$$

The operators $\hat{Q}_d(\tau_d)$ and $\hat{\Phi}_d(x_d)$ are expanded by the mode functions and the creation(annihilation) operators as

$$\hat{Q}_i(\tau_i) = \sqrt{\frac{\hbar}{2\Omega_r}} \sum_j \left[q_i^{(j)}(\tau_i) \hat{a}_j + q_i^{(j)*}(\tau_i) \hat{a}_j^\dagger \right] + \int \frac{d^3 k}{(2\pi)^3} \sqrt{\frac{\hbar}{2\omega}} \left[q_i^{(+)}(\tau_i, \mathbf{k}) \hat{v}_\mathbf{k} + q_i^{(-)}(\tau_i, \mathbf{k}) \hat{v}_\mathbf{k}^\dagger \right], \quad (10)$$

$$\hat{\Phi}(x) = \sqrt{\frac{\hbar}{2\Omega_r}} \sum_j \left[f^{(j)}(x) \hat{a}_j + f^{(j)*}(x) \hat{a}_j^\dagger \right] + \int \frac{d^3 k}{(2\pi)^3} \sqrt{\frac{\hbar}{2\omega}} \left[f^{(+)}(x, \mathbf{k}) \hat{v}_\mathbf{k} + f^{(-)}(x, \mathbf{k}) \hat{v}_\mathbf{k}^\dagger \right], \quad (11)$$

where $i, j = A, B$, $\tau_A = t$, $\tau_B = \tau$, $q_i^{(j)}$, $q_i^{(\pm)}$, $f^{(j)}$ and $f^{(\pm)}$ are the c-number mode functions. The conjugate momenta are $\hat{P}_A(t) = \partial_t \hat{Q}_A(t)$, $\hat{P}_B(\tau) = \partial_\tau \hat{Q}_B(\tau)$, and $\hat{\Pi}(x) = \partial_t \hat{\Phi}(x)$. The equations of motion for the mode functions are the following

$$(\partial_{\tau_i}^2 + \Omega_0^2) q_i^{(j)}(\tau_i) = \lambda_0 f^{(j)}(z_i^\mu(\tau_i)), \quad (12)$$

$$(\partial_t^2 - \nabla^2) f^{(j)}(x) = \lambda_0 \left[\int_0^\infty dt q_A^{(j)} \delta^4(x - z_A(t)) + \int_0^\infty d\tau q_B^{(j)} \delta^4(x - z_B(\tau)) \right], \quad (13)$$

$$(\partial_{\tau_i}^2 + \Omega_0^2) q_i^{(+)}(\tau_i, \mathbf{k}) = \lambda_0 f^{(+)}(z_i^\mu(\tau_i), \mathbf{k}), \quad (14)$$

$$\begin{aligned} (\partial_t^2 - \nabla^2) f^{(+)}(x, \mathbf{k}) = \lambda_0 & \left[\int_0^\infty dt q_A^{(+)}(t, \mathbf{k}) \delta^4(x - z_A(t)) \right. \\ & \left. + \int_0^\infty d\tau q_B^{(+)}(\tau, \mathbf{k}) \delta^4(x - z_B(\tau)) \right], \end{aligned} \quad (15)$$

in the future work, we would like to study the issues about quantum teleportation after we obtain the solutions for \hat{Q}_A and \hat{Q}_B in this model. In the present work, for simplicity and a clear picture, we will first look at the two-point functions of the moving detector Bob solely. We will consider two different kinds of trajectories for Bob–(i) Bob is uniformly accelerated and (ii) Bob moves at constant velocity. By calculating the solutions and the two-point correlation functions for the detector Bob under these two types of trajectories, we will understand the feature of acceleration and the feature of inertial motion so that we can apply these results to the future applications.

III. TWO-POINT FUNCTIONS FOR A MOVING DETECTOR

We focus on the moving detector Bob.

1. Moving Detector Bob

For simplicity, when we just consider the moving detector Bob, we may temporary ignore the other static detector Alice in the action S in Eq. (1), then the action has only Q_B part is the following

$$S = - \int d^4x \sqrt{-g} \frac{1}{2} \partial_\mu \Phi(x) \partial^\mu \Phi(x) + \int d\tau_B \frac{m_0}{2} \left[(\partial_B Q_B)^2 - \Omega_0^2 Q_B^2 \right] + \lambda_0 \int d^4x \int d\tau_B Q_B(\tau_B) \Phi(x) \delta^4(x^\mu - z_B^\mu(\tau_B)). \quad (16)$$

The Heisenberg equations for the operators and the fields can be wrote down in the following form[21](we take $\hat{Q}_B = \hat{Q}$ from now on, and also we take $m_0 = 1$ in the numerical calculation later)

$$\partial_\tau^2 \hat{Q}(\tau) + \Omega_0^2 \hat{Q}(\tau) = \lambda_0 \hat{\Phi}(\tau, \mathbf{z}(\tau)), \quad (17)$$

$$(\partial_t^2 - \nabla^2) \hat{\Phi}(x) = \lambda_0 \int_0^\infty d\tau \hat{Q}(\tau) \delta^4(x - z(\tau)). \quad (18)$$

Assuming the system is prepared before $\tau = 0$, and the coupling is turned on at $\tau = 0$ when we allow all the dynamical variables begin to interact and evolve under the influence of each other. The time evolution of $\hat{\Phi}(x)$ is a linear transformation in the phase space spanned by the orthonormal basis $(\hat{\Phi}(\mathbf{x}), \hat{\Pi}(\mathbf{x}), \hat{Q}, \hat{P})$, and $\hat{\Phi}(x)$ can be expressed in the form

$$\hat{\Phi}(t, \mathbf{x}) = \int d^3x' \left[f^\Phi(t, \mathbf{x}, \mathbf{x}') \hat{\Phi}(0, \mathbf{x}') + f^\Pi(t, \mathbf{x}, \mathbf{x}') \hat{\Pi}(0, \mathbf{x}') \right] + f^Q(x) \hat{Q}(0) + f^P(x) \hat{P}(0). \quad (19)$$

Here $f^\Phi(x, \mathbf{x}')$, $f^\Pi(x, \mathbf{x}')$, $f^Q(x)$ and $f^P(x)$ are c-number functions. Similarly, the operator $\hat{Q}(\tau)$ can be expressed in the following

$$\hat{Q}(\tau) = \int d^3x' \left[q^\Phi(\tau, \mathbf{x}') \hat{\Phi}(0, \mathbf{x}') + q^\Pi(\tau, \mathbf{x}') \hat{\Pi}(0, \mathbf{x}') \right] + q^Q(\tau) \hat{Q}(0) + q^P(\tau) \hat{P}(0), \quad (20)$$

with c-number functions $q^Q(\tau)$, $q^P(\tau)$, $q^\Phi(\tau, \mathbf{x}')$ and $q^\Pi(\tau, \mathbf{x}')$.

For the case with initial operators being the free field operators, namely, $\hat{\Phi}(0, \mathbf{x}) = \hat{\Phi}_0(\mathbf{x})$, $\hat{\Pi}(0, \mathbf{x}) = \hat{\Pi}_0(\mathbf{x})$, $\hat{Q}(0) = \hat{Q}_0$ and $\hat{P}(0) = \hat{P}_0$, one can go further by introducing the complex operators $\hat{v}_\mathbf{k}$ and \hat{a} :

$$\hat{\Phi}_0(\mathbf{x}) = \int \frac{d^3k}{(2\pi)^3} \sqrt{\frac{\hbar}{2\omega}} \left[e^{i\mathbf{k}\cdot\mathbf{x}} \hat{v}_\mathbf{k} + e^{-i\mathbf{k}\cdot\mathbf{x}} \hat{v}_\mathbf{k}^\dagger \right], \quad (21)$$

$$\hat{\Pi}_0(\mathbf{x}) = \int \frac{d^3k}{(2\pi)^3} \sqrt{\frac{\hbar}{2\omega}} (-i\omega) \left[e^{i\mathbf{k}\cdot\mathbf{x}} \hat{v}_\mathbf{k} - e^{-i\mathbf{k}\cdot\mathbf{x}} \hat{v}_\mathbf{k}^\dagger \right] \quad (22)$$

with $\omega \equiv |\mathbf{k}|$, and

$$\hat{Q}_0 = \sqrt{\frac{\hbar}{2\Omega_r m_0}} (\hat{a} + \hat{a}^\dagger), \quad \hat{P}_0 = -i\sqrt{\frac{\hbar\Omega_r m_0}{2}} (\hat{a} - \hat{a}^\dagger). \quad (23)$$

Note that, instead of Ω_0 , we use the renormalized natural frequency Ω_r (to be defined in Eq. (84)) in the definition of \hat{a} . Then the commutation relations (6) and (7) give

$$[\hat{a}, \hat{a}^\dagger] = 1, \quad [\hat{v}_\mathbf{k}, \hat{v}_{\mathbf{k}'}^\dagger] = (2\pi)^3 \delta^3(\mathbf{k} - \mathbf{k}'), \quad (24)$$

and the expressions (19) and (20) can be re-written as

$$\hat{\Phi}(t, \mathbf{x}) = \hat{\Phi}_v(x) + \hat{\Phi}_a(x), \quad (25)$$

$$\hat{Q}(\tau) = \hat{Q}_v(\tau) + \hat{Q}_a(\tau) \quad (26)$$

where

$$\hat{\Phi}_v(x) = \int \frac{d^3 k}{(2\pi)^3} \sqrt{\frac{\hbar}{2\omega}} \left[f^{(+)}(t, \mathbf{x}; \mathbf{k}) \hat{v}_\mathbf{k} + f^{(-)}(t, \mathbf{x}; \mathbf{k}) \hat{v}_\mathbf{k}^\dagger \right], \quad (27)$$

$$\hat{\Phi}_a(x) = \sqrt{\frac{\hbar}{2\Omega_r m_0}} \left[f^a(t, \mathbf{x}) \hat{a} + f^{a*}(t, \mathbf{x}) \hat{a}^\dagger \right], \quad (28)$$

$$\hat{Q}_v(\tau) = \int \frac{d^3 k}{(2\pi)^3} \sqrt{\frac{\hbar}{2\omega}} \left[q^{(+)}(\tau, \mathbf{k}) \hat{v}_\mathbf{k} + q^{(-)}(\tau, \mathbf{k}) \hat{v}_\mathbf{k}^\dagger \right], \quad (29)$$

$$\hat{Q}_a(\tau) = \sqrt{\frac{\hbar}{2\Omega_r m_0}} \left[q^a(\tau) \hat{a} + q^{a*}(\tau) \hat{a}^\dagger \right]. \quad (30)$$

The whole problem therefore can be transformed to solving c-number functions $f(x)$ and $q(\tau)$ from (17) and (18) with suitable initial conditions. Since \hat{Q} and $\hat{\Phi}$ are hermitian, one has $f^{(-)} = (f^{(+)})^*$ and $q^{(-)} = (q^{(+)})^*$. Hence it is sufficient to solve the c-number functions $f^{(+)}(t, \mathbf{x}; \mathbf{k})$, $q^{(+)}(\tau, \mathbf{k})$, $f^a(t, \mathbf{x})$ and $q^a(\tau)$. To place this in a more general setting, let us perform a Lorentz transformation shifting $\tau = 0$ to $\tau = \tau_0$, and define

$$\eta \equiv \tau - \tau_0. \quad (31)$$

Now the coupling between the detector and the field would be turned on at $\tau = \tau_0$. We are looking for solutions with the initial conditions as the following

$$f^{(+)}(t(\tau_0), \mathbf{x}; \mathbf{k}) = e^{i\mathbf{k}\cdot\mathbf{x}}, \quad \partial_t f^{(+)}(t(\tau_0), \mathbf{x}; \mathbf{k}) = -i\omega e^{i\mathbf{k}\cdot\mathbf{x}}, \quad q^{(+)}(\tau_0; \mathbf{k}) = \dot{q}^{(+)}(\tau_0; \mathbf{k}) = 0, \quad (32)$$

$$f^a(t(\tau_0), \mathbf{x}) = \partial_t f^a(t(\tau_0), \mathbf{x}) = 0, \quad q^a(\tau_0) = 1, \quad \dot{q}^a(\tau_0) = -i\Omega_r. \quad (33)$$

2. Solutions for detector Bob

The solutions for $f_0^{(+)}$, $f^{(+)}$, $q^{(+)}$, f^a and q^a are list in the following (detail calculations are wrote down in Appendix A)

The general solution for $f^{(+)}$ reads

$$f^{(+)}(x; \mathbf{k}) = f_0^{(+)}(x; \mathbf{k}) + f_1^{(+)}(x; \mathbf{k}), \quad (34)$$

where

$$f_0^{(+)}(x; \mathbf{k}) \equiv e^{-i\omega t + i\mathbf{k}\cdot\mathbf{x}} \quad (35)$$

is the free field solution.

$$f_1^{(+)}(z(\tau); \mathbf{k}) = \frac{\lambda_0}{4\pi} \left[\Lambda \zeta q^{(+)}(\tau; \mathbf{k}) - \partial_\tau q^{(+)}(\tau; \mathbf{k}) + O(\Lambda^{-1}) \right], \quad (36)$$

where $\zeta = 2^{7/4} \Gamma(5/4) / \sqrt{\pi}$ and Λ is about the regularization scheme.

$$q^{(+)}(\tau; \mathbf{k}) = \frac{\lambda_0}{m_0} \sum_{j=+,-} \int_{\tau_0}^{\tau} d\tau' c_j e^{w_j(\tau-\tau')} f_0^{(+)}(z(\tau'); \mathbf{k}), \quad (37)$$

where $c_\pm = \pm \frac{1}{2i\Omega}$, $w_\pm = -\gamma \pm i\Omega$, with $\Omega \equiv \sqrt{\Omega_r^2 - \gamma^2}$.

$$f^a(x) = \frac{\lambda_0 \theta(\eta_-)}{2\pi a X} q^a(\tau_-). \quad (38)$$

and

$$q^a(\tau) = \frac{1}{2} \theta(\eta) e^{-\gamma\eta} \left[\left(1 - \frac{\Omega_r + i\gamma}{\Omega} \right) e^{i\Omega\eta} + \left(1 + \frac{\Omega_r + i\gamma}{\Omega} \right) e^{-i\Omega\eta} \right]. \quad (39)$$

where X is defined in Appendix A.

Above is the general form of the solutions. The explicit solutions will depend on the specific worldline of the detector (the trajectory for the moving detector in spacetime). Later, we will compute the solutions for two different kinds of trajectories for the moving detector.

3. States for the detector and field

As shown in the previous section, when \hat{Q} evolves, some non-zero terms proportional to $\hat{\Phi}$ and \hat{H} will be generated. Suppose the detector is initially prepared in a state that can be factorized into the quantum state $|q\rangle$ for Q and the Minkowski vacuum $|0_M\rangle$ for the scalar field Φ , that is,

$$|\tau_0\rangle = |q\rangle |0_M\rangle \quad (40)$$

then the two-point function of Q will split into two parts,

$$\begin{aligned} \langle Q(\tau)Q(\tau') \rangle &= \langle 0_M | \langle q | [\hat{Q}_v(\tau) + \hat{Q}_a(\tau)] [\hat{Q}_v(\tau) + \hat{Q}_a(\tau)] | q \rangle | 0_M \rangle \\ &= \langle q | q \rangle \langle Q(\tau)Q(\tau') \rangle_v + \langle Q(\tau)Q(\tau') \rangle_a \langle 0_M | 0_M \rangle. \end{aligned} \quad (41)$$

where, from Eq. (26),

$$\langle Q(\tau)Q(\tau') \rangle_v = \langle 0_M | \hat{Q}_v(\tau) \hat{Q}_v(\tau') | 0_M \rangle, \quad (42)$$

$$\langle Q(\tau)Q(\tau') \rangle_a = \langle q | \hat{Q}_a(\tau) \hat{Q}_a(\tau) | q \rangle. \quad (43)$$

Similar splitting happens for every two-point function of $\hat{\Phi}(x)$ as well as for the stress-energy tensor.

Observe that $\langle Q(\tau)Q(\tau') \rangle_v$ depends on the initial state of the field, or the Minkowski vacuum, while $\langle Q(\tau)Q(\tau') \rangle_a$ depends on the initial state of the detector only. One can thus interpret $\langle Q(\tau)Q(\tau') \rangle_v$ as accounting for the response to the vacuum fluctuations, while $\langle Q(\tau)Q(\tau') \rangle_a$ corresponds to the intrinsic quantum fluctuations in the detector.

In the following, we will focus on the $\langle Q(\tau)Q(\tau') \rangle_v$ part (response to the vacuum fluctuations) and demonstrate the explicit forms of the two-point correlation functions.

4. Trajectory 1 : Two-point function for UAD

Here we investigate the two-point correlation function for the uniformly accelerated detector(UAD) Bob who is along the trajectory $z_B^\mu = (a^{-1} \sinh a\tau, a^{-1} \cosh a\tau, 0, 0)$ with $a \neq 0$.

The two-point function $\langle Q(\tau - \tau_0)Q(\tau'' - \tau_0'') \rangle_v$ for Bob is the following

$$\begin{aligned} &\langle Q(\tau - \tau_0)Q(\tau'' - \tau_0'') \rangle_v \\ &= \hbar \int_{-\infty}^{\infty} \frac{d^3 k}{(2\pi)^3 2\omega} q^{(+)}(\tau; \mathbf{k}) q^{(-)}(\tau; \mathbf{k}) \\ &= \frac{\hbar}{2\omega} \int \frac{d^3 \vec{k}}{(2\pi)^3} \frac{\lambda_0}{m_0} \sum_{j=+,-} \int_{\tau_0}^{\tau} d\tau' c_j e^{w_j(\tau - \tau')} f_0^{(+)}(z(\tau'), \vec{k}) \\ &\quad \cdot \frac{\lambda_0}{m_0} \sum_{j=+,-} \int_{\tau_0}^{\tau''} d\tau''' c_j^* e^{w_j^*(\tau'' - \tau''')} f_0^{*(+)}(z(\tau'''), \vec{k}), \end{aligned} \quad (44)$$

then perform Fourier Transform to $f_0^{(+)}$

$$f_0^{(+)}(z(\tau'), \vec{k}) = \int d\kappa e^{-i\kappa\tau'} \varphi_{\vec{k}}(\kappa), \quad (45)$$

the above two-point function is expressed in the form below

$$\begin{aligned} &\langle Q(\tau - \tau_0)Q(\tau'' - \tau_0'') \rangle_v \\ &= \frac{\lambda_0^2}{m_0^2} \sum_{j,j'=+,-} \int_{\tau_0}^{\tau} d\tau' c_j e^{w_j(\tau - \tau')} \int d\kappa e^{-i\kappa\tau'} \int_{\tau_0''}^{\tau''} d\tau''' c_{j'}^* e^{w_{j'}^*(\tau'' - \tau''')} \int d\kappa' e^{-i\kappa'\tau'''} \\ &\quad \cdot F. \end{aligned} \quad (46)$$

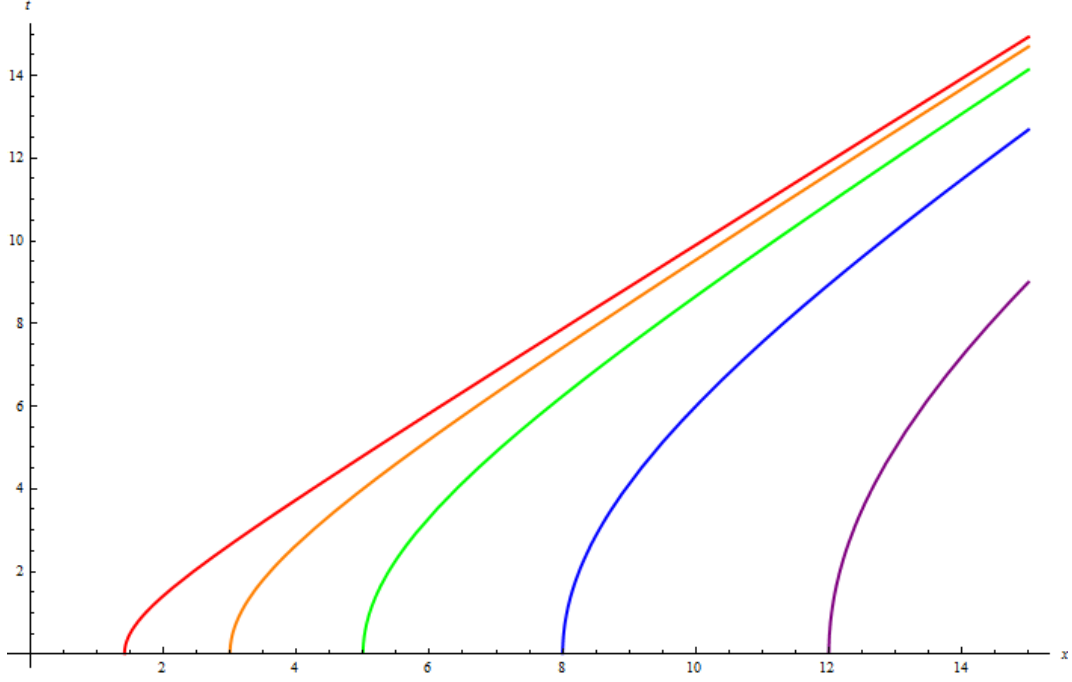


FIG. 1: The plot for the worldline $z_B^\mu = (a^{-1} \sinh a\tau, a^{-1} \cosh a\tau, 0, 0)$ for different proper acceleration value a . As the proper acceleration $a \rightarrow 0$, the worldline is shifted to far away. The proper acceleration for the red line is the largest among all lines while the proper acceleration for the purple line is the smallest among all lines.

Where F is defined as

$$F \equiv \frac{\hbar}{2\omega} \int_{-\infty}^{\infty} \frac{d^3 k}{2\pi} \varphi_{\vec{k}}(\kappa) \varphi_{\vec{k}}^*(\kappa') . \quad (47)$$

The Fourier factor $\varphi_{\vec{k}}(\kappa)$ is

$$\varphi_{\vec{k}}(\kappa) = \int_{-\infty}^{\infty} \frac{d\tau}{2\pi} e^{-i\omega z^0(\tau) + i\vec{k} \cdot \vec{z}(\tau)} , \quad (48)$$

then F is the following

$$\begin{aligned} F &= \frac{\hbar}{(2\pi)^3} \int_0^{2\pi} d\phi \int_{-1}^1 d(\cos \theta) \int_0^{\infty} \frac{\omega^2 d\omega}{2\omega} \int_{-\infty}^{+\infty} \frac{dt}{2\pi} \int_{-\infty}^{+\infty} \frac{dt'}{2\pi} e^{i\kappa t - i\kappa' t' - i\omega(z^0(t) - z^0(t') + i\omega \cos \theta |\vec{z} - \vec{z}'|)} \\ &= \frac{\hbar}{2\pi} \int_0^{\infty} d\omega \int_{-\infty}^{+\infty} \frac{dt}{2\pi} \int_{-\infty}^{+\infty} \frac{dt'}{2\pi} e^{i\kappa t - i\kappa' t' - i\omega[z^0(t) - z^0(t')]} \frac{\sin(\omega |\vec{z}(t) - \vec{z}(t')|)}{|\vec{z}(t) - \vec{z}(t')|} \\ &= \frac{\hbar}{(2\pi)^4} \lim_{\epsilon \rightarrow 0} \int_{-\infty}^{+\infty} dt \int_{-\infty}^{+\infty} dt' \frac{e^{i\kappa(t - \frac{i\epsilon}{2}) - i\kappa'(t' + \frac{i\epsilon}{2})}}{|\vec{z}(t - \frac{i\epsilon}{2}) - \vec{z}(t' + \frac{i\epsilon}{2})|^2 - [z^0(t - \frac{i\epsilon}{2}) - z^0(t + \frac{i\epsilon}{2})]^2} \\ &= \frac{\hbar}{(2\pi)^4} \lim_{\epsilon \rightarrow 0} \int_{-\infty}^{+\infty} dt \int_{-\infty}^{+\infty} dt' \frac{a^2 e^{\frac{\epsilon}{2}(\kappa + \kappa') + i\kappa t - i\kappa' t'}}{-4 \sinh^2(\frac{a}{2}((t - t') - i\epsilon))} \\ &= \frac{\hbar}{(2\pi)^4} \lim_{\epsilon \rightarrow 0} \int_{-\infty}^{+\infty} dT \int_{-\infty}^{+\infty} d\Delta \frac{a^2 e^{\frac{\epsilon}{2}(\kappa + \kappa') + i(\kappa - \kappa')T + \frac{i\Delta}{2}(\kappa + \kappa')}}{-4 \sinh^2(\frac{a}{2}(\Delta - i\epsilon))} \\ &= \frac{\hbar a^2}{(2\pi)^3} \delta(\kappa - \kappa') \lim_{\epsilon \rightarrow 0} \int_{-\infty}^{+\infty} d\Delta \frac{e^{\kappa\epsilon} e^{i\kappa\Delta}}{-4 \sinh^2 \frac{a}{2}(\Delta - i\epsilon)} , \end{aligned} \quad (49)$$

in the above third line, we take $t \rightarrow t - \frac{i\epsilon}{2}$ to suppress the contribution from high-frequency modes of the field and this equal to set a finite time resolution of the system. And then in the above fifth line we take $T \equiv \frac{t+t'}{2}$ and $\Delta \equiv t - t'$,

the integral is a double complex integral. Note that there are poles at $\frac{a}{2}(\Delta - i\epsilon) = \pm i\bar{n}$ where $\bar{n} = 0, 1, 2, 3, \dots, \infty$. Then, we plug F back to the two-point function $\langle Q(\tau - \tau_0)Q(\tau'' - \tau_0'') \rangle_v$ and then perform the integration of τ , thus we have the form in the following

$$\begin{aligned}
& \langle Q(\tau - \tau_0)Q(\tau'' - \tau_0'') \rangle_v \\
&= \frac{\lambda_0^2}{m_0^2} \sum_{j,j'=\pm,-} \int_{\tau_0}^{\tau} d\tau' c_j e^{w_j(\tau - \tau')} \int_{-\infty}^{+\infty} d\kappa e^{-i\kappa\tau'} \int_{\tau_0'}^{\tau''} d\tau''' c_{j'}^* e^{w_{j'}^*(\tau'' - \tau''')} \int_{-\infty}^{+\infty} d\kappa' e^{i\kappa'\tau'''} \\
&\quad \cdot \frac{\hbar a^2}{(2\pi)^3} \delta(\kappa - \kappa') \lim_{\epsilon \rightarrow 0} \int_{-\infty}^{+\infty} d\Delta \frac{e^{\kappa\epsilon} e^{i\kappa\Delta}}{-4 \sinh^2 \frac{a}{2}(\Delta - i\epsilon)} \\
&= \frac{\lambda_0^2}{m_0^2} \frac{\hbar}{(2\pi)^2} \sum_{j,j'=\pm} \left(\frac{a^2}{2\pi} \right) \lim_{\epsilon \rightarrow 0} \left[\int_0^{\infty} d\kappa e^{-i\kappa(\tau_0 - \tau_0'')} \int_{-\infty}^{+\infty} d\Delta \frac{e^{\kappa\epsilon} e^{i\kappa\Delta}}{-4 \sinh^2 \frac{a}{2}(\Delta - i\epsilon)} \right. \\
&\quad \left. + \int_{-\infty}^0 d\kappa e^{-i\kappa(\tau_0 - \tau_0'')} \int_{-\infty}^{+\infty} d\Delta \frac{e^{\kappa\epsilon} e^{i\kappa\Delta}}{-4 \sinh^2 \frac{a}{2}(\Delta + i\epsilon)} \right] \\
&\quad \cdot \frac{c_j c_{j'}^* (e^{w_j(\tau - \tau_0)} - e^{i\kappa(\tau_0 - \tau)})(e^{w_{j'}^*(\tau'' - \tau_0'')} - e^{i\kappa(\tau'' - \tau_0'')})}{(w_j + i\kappa)(w_{j'}^* - i\kappa)} \\
&= \frac{2\lambda_0^2 \hbar}{(2\pi)^2 m_0^2} \sum_{j,j'} \int_0^{\infty} \frac{\kappa d\kappa}{1 - e^{-2\pi\kappa/a}} \frac{c_j c_{j'}^* e^{-i\kappa(\tau_0 - \tau_0'')}}{(w_j + i\kappa)(w_{j'}^* - i\kappa)} (e^{w_j(\tau - \tau_0)} - e^{-i\kappa(\tau - \tau_0)}) \\
&\quad \cdot (e^{w_{j'}^*(\tau'' - \tau_0'')} - e^{i\kappa(\tau'' - \tau_0'')}), \tag{50}
\end{aligned}$$

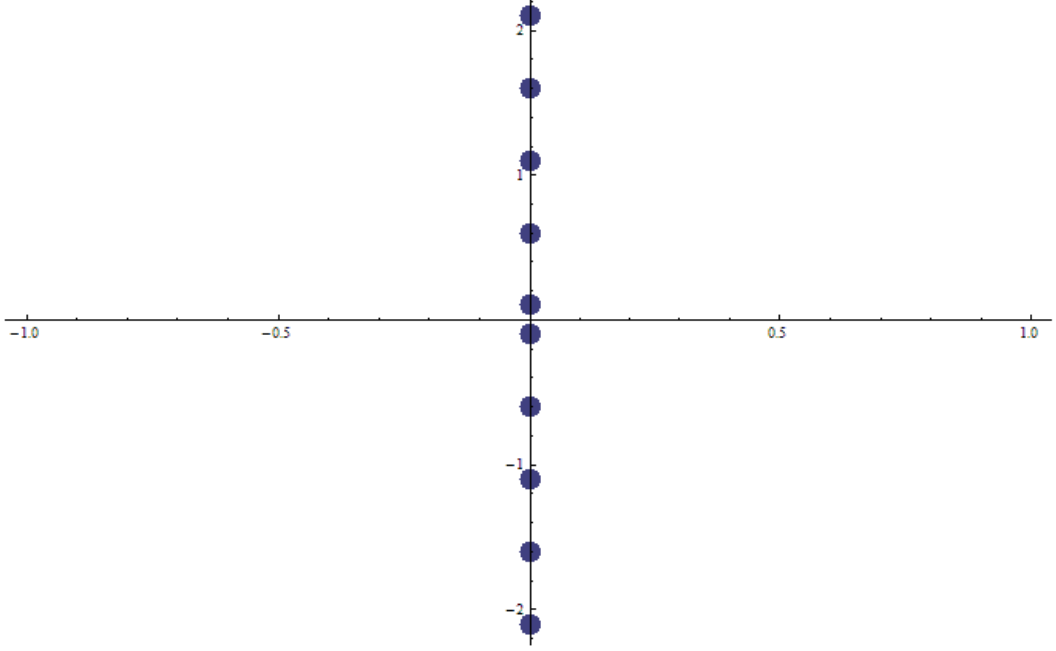


FIG. 2: Poles on the complex Δ plane at $\Delta = i(\epsilon + \frac{2\pi\bar{n}}{a})$ on the upper complex plane and at $\Delta = -i(\epsilon + \frac{2\pi\bar{n}}{a})$ on the lower complex plane. Where $\bar{n} = 0, 1, 2, 3, \dots, \infty$, the poles move to $\pm i\infty$ as $a \rightarrow 0$.

Now, the integrals in the second equal sign of Eq.(50) is the tricky part (the double complex integrals). Note that inside the square brackets of Eq.(50), the κ and Δ double integral is split into two parts because the sign of κ determine the contour integration is performed on the upper half complex plane or on the lower half plane. The first term in Eq.(51), the Δ contour integral circle on the upper plane when $\kappa > 0$, while the second term Δ contour integral circle on the lower plane when $\kappa < 0$. If we didn't notice this point, we would have just one term and ignore the other term as in the past results.

$$\int_0^\infty d\kappa e^{-i\kappa(\tau' - \tau''')} \int_{-\infty}^{+\infty} d\Delta \frac{e^{\kappa\epsilon} e^{i\kappa\Delta}}{-4 \sinh^2 \frac{a}{2}(\Delta - i\epsilon)} + \int_{-\infty}^0 d\kappa e^{-i\kappa(\tau' - \tau''')} \int_{-\infty}^{+\infty} d\Delta \frac{e^{\kappa\epsilon} e^{i\kappa\Delta}}{-4 \sinh^2 \frac{a}{2}(\Delta + i\epsilon)}. \quad (51)$$

There are poles in the denominator $\sinh^2 \frac{a}{2}(\Delta - i\epsilon)$ at $\Delta = i(\epsilon + \frac{2\pi\bar{n}}{a})$ and poles in the other denominator $\sinh^2 \frac{a}{2}(\Delta + i\epsilon)$ at $\Delta = -i(\epsilon + \frac{2\pi\bar{n}}{a})$. We may use the identity

$$\csc^2 \pi x = \frac{1}{\pi^2} \sum_{n=-\infty}^{\infty} \frac{1}{(x - n)^2}, \quad (52)$$

and the relation $\sinh^2 x = -\sin^2(ix)$ to expand those poles.

We expand $\sinh x$ in the first integral such that

$$\frac{-1}{4 \sinh^2 \frac{a}{2}(\Delta - i\epsilon)} = \frac{1}{4 \sin^2(\frac{ia\Delta}{2} + \epsilon)} = \frac{-1}{a^2} \sum_{n=-\infty}^{\infty} \frac{1}{(\Delta - i\epsilon + i2\pi n/a)^2}. \quad (53)$$

In the first integral(Eq.(51)), only the poles $n = 0, -1, -2, \dots, -\infty$ are inside the contour, let $\bar{n} = -n$ the first integral is reexpressed in following

$$\begin{aligned} & \int_0^\infty d\kappa e^{-i\kappa(\tau' - \tau''')} \int_{-\infty}^{+\infty} d\Delta \frac{e^{\kappa\epsilon} e^{i\kappa\Delta}}{-4 \sinh^2 \frac{a}{2}(\Delta - i\epsilon)} \\ &= \int_0^\infty d\kappa e^{-i\kappa(\tau' - \tau''')} \int_{-\infty}^{+\infty} d\Delta \sum_{\bar{n}=0}^{\infty} \frac{e^{\kappa\epsilon} e^{i\kappa\Delta}}{-a^2 [\Delta - i(\epsilon + 2\pi\bar{n}/a)]^2}, \end{aligned} \quad (54)$$

where some term 2π and n are absorbed into ϵ . Similarly, the second integral(Eq.(51)) is expanded as the same way

$$\frac{-1}{4 \sinh^2 \frac{a}{2}(\Delta + i\epsilon)} = \frac{1}{4 \sin^2(\frac{ia\Delta}{2} - \epsilon)} = \frac{-1}{a^2} \sum_{n=-\infty}^{\infty} \frac{1}{(\Delta + i\epsilon + i2\pi n/a)^2}. \quad (55)$$

Only the poles $n = 0, 1, 2, \dots, \infty$ are inside the contour of the second integral. Therefore, the second integral is reexpressed in the following

$$\begin{aligned} & \int_{-\infty}^0 d\kappa e^{-i\kappa(\tau' - \tau''')} \int_{-\infty}^{+\infty} d\Delta \frac{e^{\kappa\epsilon} e^{i\kappa\Delta}}{-4 \sinh^2 \frac{a}{2}(\Delta + i\epsilon)} \\ &= \int_{-\infty}^0 d\kappa e^{-i\kappa(\tau' - \tau''')} \int_{-\infty}^{+\infty} d\Delta \sum_{n=0}^{\infty} \frac{e^{\kappa\epsilon} e^{i\kappa\Delta}}{-a^2 [\Delta + i(\epsilon + 2\pi n/a)]^2}, \end{aligned} \quad (56)$$

In our space-time diagram $a \leq 1$ (we assume the light speed $c = 1$ thus the proper acceleration $a \leq 1$), note that when $a \rightarrow 0$ the poles on the complex Δ plane move to ∞ and the arc integration $\int_{arc} d\Delta f(\Delta)$ in Cauchy's integral formula no longer be 0(the arc can not include the poles when the poles move to ∞), the integral is ill-defined. And if we think carefully, back to Figure 1 and check the worldline for the detector Bob, we can see that as $a \rightarrow 0$, Bob is very very far away toward ∞ thus Bob can not exchange the signal with Alice in a finite time interval, this situation is not the proper set up we want (we need Alice and Bob are separated by some proper distance that they can exchange signal to each other in a reasonable time interval so that we can study the properties in the quantum teleportation process for such set up in the future work). Therefore, the result when $a \rightarrow 0$ in Eq.(51) is not the real set up that it can be extended to the case that Alice and Bob have finite distance between them and exchange signals when Bob moves at constant velocity.

Plugging Eq.(54) and Eq.(56) back to Eq.(50) we have

$$\frac{-1}{a^2} \lim_{\epsilon \rightarrow 0} \left(\int_0^\infty d\kappa \int_{-\infty}^{\infty} d\Delta \sum_{\bar{n}=0}^{\infty} \frac{e^{\kappa\epsilon} e^{i\kappa\Delta}}{[\Delta - i(\epsilon + \frac{2\pi\bar{n}}{a})]^2} + \int_{-\infty}^0 d\kappa \int_{-\infty}^{\infty} d\Delta \sum_{\bar{n}=0}^{\infty} \frac{e^{\kappa\epsilon} e^{i\kappa\Delta}}{[\Delta + i(\epsilon + \frac{2\pi\bar{n}}{a})]^2} \right), \quad (57)$$

then, perform the Δ integration(taking $\epsilon = 0$ in the end) , we have the following

$$\begin{aligned} & \frac{-1}{a^2} \left(\int_0^\infty d\kappa \sum_{\bar{n}=0}^\infty (2\pi i) i\kappa e^{i\kappa i(+\frac{2\pi\bar{n}}{a})} + \int_{-\infty}^0 d\kappa \sum_{\bar{n}=0}^\infty (-2\pi i) i\kappa e^{i\kappa i(-\frac{2\pi\bar{n}}{a})} \right) \\ &= \frac{-1}{a^2} \left(\int_0^\infty d\kappa \sum_{\bar{n}=0}^\infty (2\pi i) i\kappa e^{i\kappa i(\frac{2\pi\bar{n}}{a})} - \int_{-\infty}^0 d\kappa \sum_{\bar{n}=0}^\infty (2\pi i) i\kappa e^{-i\kappa i(\frac{2\pi\bar{n}}{a})} \right). \end{aligned} \quad (58)$$

Then, plugging the above result back to Eq.(50), we obtain the following term

$$\begin{aligned} & \frac{-1}{a^2} \left(\int_0^\infty d\kappa \sum_{\bar{n}=0}^\infty (2\pi i) i\kappa e^{i\kappa i(\frac{2\pi\bar{n}}{a})} - \int_{-\infty}^0 d\kappa \sum_{\bar{n}=0}^\infty (2\pi i) i\kappa e^{-i\kappa i(\frac{2\pi\bar{n}}{a})} \right) e^{-i\kappa(\tau_0 - \tau_0'')} \\ & \cdot \frac{C_j C_{j'}^* (e^{w_j(\tau - \tau_0)} - e^{i\kappa(\tau_0 - \tau)})(e^{w_{j'}^*(\tau'' - \tau_0'')} - e^{i\kappa(\tau'' - \tau_0'')})}{(w_j + i\kappa)(w_{j'}^* - i\kappa)} \\ &= \frac{-1}{a^2} \left[\int_0^\infty d\kappa \sum_{\bar{n}=0}^\infty X^{\bar{n}} F(\kappa) - \int_{-\infty}^0 d\kappa \sum_{\bar{n}=0}^\infty X^{-\bar{n}} F(\kappa) \right], \end{aligned} \quad (59)$$

where $X^{\bar{n}} = e^{-\kappa \frac{2\pi}{a}}$ and $F(\kappa) = (2\pi i) i\kappa \cdot \frac{C_j C_{j'}^* (e^{w_j(\tau - \tau_0)} - e^{i\kappa(\tau_0 - \tau)})(e^{w_{j'}^*(\tau'' - \tau_0'')} - e^{i\kappa(\tau'' - \tau_0'')}) e^{-i\kappa(\tau_0 - \tau_0'')} }{(w_j + i\kappa)(w_{j'}^* - i\kappa)}.$

Note that there are many poles on the imaginary axis of κ complex plane, it is difficult to do contour integration in the form of Eq.(59). To avoid the difficulty of such contour integral, we can reshape Eq.(59) in the following way to avoid the poles

$$\begin{aligned} & \frac{-1}{a^2} \left[\int_0^\infty dk \sum_{\bar{n}=0}^\infty X^{\bar{n}} - \int_{-\infty}^0 dk \sum_{\bar{n}=0}^\infty X^{-\bar{n}} \right] F(\kappa) \\ &= \frac{-1}{a^2} \left[\int_0^\infty d\kappa \frac{1}{1 - X} - \int_{-\infty}^0 d\kappa \frac{1}{1 - X^{-1}} \right] F(\kappa) \\ &= \frac{-1}{a^2} \left[\int_0^\infty d\kappa \frac{1}{1 - X} - \int_{-\infty}^0 d\kappa \frac{X}{X - 1} \right] F(\kappa) \\ &= \frac{-1}{a^2} \left[\int_0^\infty d\kappa \frac{1}{1 - X} + \int_{-\infty}^0 d\kappa \frac{X - 1 + 1}{1 - X} \right] F(\kappa) \\ &= \frac{-1}{a^2} \left[\int_0^\infty d\kappa \frac{1}{1 - X} + \int_{-\infty}^0 d\kappa \frac{1}{1 - X} + \int_{-\infty}^0 d\kappa \frac{X - 1}{1 - X} \right] F(\kappa) \\ &= \frac{-1}{a^2} \left[\int_{-\infty}^\infty \frac{d\kappa F(\kappa)}{1 - X} - \int_{-\infty}^0 d\kappa F(\kappa) \right]. \end{aligned} \quad (60)$$

By the trick above(we rewrite the integral region from $-\infty$ to ∞ and include the poles inside the contour in the first integral) , the difficult contour integral from 0 to ∞ is prevented.

Then, we plug the above results back to Eq.(50), thus the two-point function Eq.(50) is reshaped as the following

$$\begin{aligned} & \langle Q(\tau - \tau_0) Q(\tau'' - \tau_0'') \rangle_v \\ &= \frac{\lambda_0^2 \hbar}{m_0^2 (2\pi)^2} \left[\sum_{j, j'=\pm} C_j C_{j'}^* \int_{-\infty}^\infty \frac{\kappa d\kappa e^{-i\kappa(\tau_0 - \tau_0'')}(e^{w_j(\tau - \tau_0)} - e^{i\kappa(\tau_0 - \tau)})(e^{w_{j'}^*(\tau'' - \tau_0'')} - e^{i\kappa(\tau'' - \tau_0'')})}{(1 - e^{-2\pi\kappa/a})(w_j + i\kappa)(w_{j'}^* - i\kappa)} \right. \\ & \quad \left. - \sum_{j, j'=\pm} C_j C_{j'}^* \int_{-\infty}^0 \frac{\kappa d\kappa e^{-i\kappa(\tau_0 - \tau_0'')}(e^{w_j(\tau - \tau_0)} - e^{i\kappa(\tau_0 - \tau)})(e^{w_{j'}^*(\tau'' - \tau_0'')} - e^{i\kappa(\tau'' - \tau_0'')})}{(w_j + i\kappa)(w_{j'}^* - i\kappa)} \right], \end{aligned} \quad (61)$$

we have two integrations in the two-point function. (The first term is the old result in the past work while the second term is the missing term in the past work.)

The steps above are the key points in the calculations. Note that $\kappa \geq 0$ is from the result of Δ contour integration(Eq.(50)). In order to avoid the difficult κ integration (many poles on the imaginary axis of κ plane) we thus reshape Eq.(50) into the form in Eq.(61). When we compare this new result with the past result, we find that the second term in Eq.(61) is missing in the past result. This is the accidentally careless when we cope with the double complex integral in Eq.(50). Also, remember that when $a = 0$, the result of this two-point function is no longer true because this result is corresponding to the situation that Bob is very far away so that Bob and Alice can not exchange message in a reasonable time interval. The mathematical reason is shown in the part of Δ contour integration , which the denominator $\sinh^2 \frac{a}{2}(\Delta - i\epsilon)$ of Δ integration in the last second line of Eq.(50) is no longer hyperbolic sine function as $a = 0$. This responds to the Figure 1 that the world line of Bob shifts to very far away as $a = 0$, and this is not the proper set up we want.

In order to compare the difference of this new result for the two-point correlation function more easily with the past one([21]), the two-point function is expressed in the following

$$\begin{aligned}
& \langle Q(\tau - \tau_0)Q(\tau'' - \tau_0'') \rangle_v \\
&= \frac{\lambda_0^2 \hbar}{(2\pi)^2 m_0^2} \sum_{j,j'} \int_0^\infty \frac{\kappa d\kappa}{1 - e^{-2\pi\kappa/a}} \frac{c_j c_{j'}^* e^{-i\kappa(\tau_0 - \tau_0'')}}{(w_j + i\kappa)(w_{j'}^* - i\kappa)} (e^{w_j(\tau - \tau_0)} - e^{-i\kappa(\tau - \tau_0)})(e^{w_{j'}^*(\tau'' - \tau_0'')} - e^{i\kappa(\tau'' - \tau_0'')}) \\
&= \frac{\lambda_0^2 \hbar}{m_0^2 (2\pi)^2} \left[\sum_{j,j'=\pm} C_j C_{j'}^* \int_{-\infty}^\infty \frac{\kappa d\kappa e^{-i\kappa(\tau_0 - \tau_0'')} (e^{w_j(\tau - \tau_0)} - e^{i\kappa(\tau - \tau_0)})(e^{w_{j'}^*(\tau'' - \tau_0'')} - e^{i\kappa(\tau'' - \tau_0'')})}{(1 - e^{-2\pi\kappa/a})(w_j + i\kappa)(w_{j'}^* - i\kappa)} \right. \\
&\quad \left. - \sum_{j,j'=\pm} C_j C_{j'}^* \int_{-\infty}^0 \frac{\kappa d\kappa e^{-i\kappa(\tau_0 - \tau_0'')} (e^{w_j(\tau - \tau_0)} - e^{i\kappa(\tau - \tau_0)})(e^{w_{j'}^*(\tau'' - \tau_0'')} - e^{i\kappa(\tau'' - \tau_0'')})}{(w_j + i\kappa)(w_{j'}^* - i\kappa)} \right] \\
&= \langle QQ \rangle_{v1} - \langle QQ \rangle_{v2}, \tag{62}
\end{aligned}$$

the first term $\langle QQ \rangle_{v1}$ is the old result in the past work([21]), and the second term $\langle QQ \rangle_{v2}$ is the missing term. The advantage that the two-point function reshaped on the above form is that it can be computed more easily, since the poles on the imaginary axis are now included inside the contour and the κ integrations can be done. Also, we can easily compare this new result with the old result([21]), and we can see the difference between the new and the old result more clearly.

Here we just write down the results of $\langle QQ \rangle_{v1}$, and $-\langle QQ \rangle_{v2}$ in Eq.(62) in the following, the detail derivations is written down in the appendix B.

$$\begin{aligned}
& \langle QQ \rangle_{v1} \\
&= \frac{2\hbar\gamma}{\pi m_0 \Omega^2} \theta(\eta) \operatorname{Re} \{ (\Lambda_0 - \ln \frac{a}{\Omega}) e^{-2\gamma\eta} \sin^2 \Omega\eta \\
&\quad + \frac{a}{2} e^{-(\gamma+a)\eta} \left[\frac{F_{\gamma+i\Omega}(e^{-a\eta})}{\gamma + i\Omega + a} \left(\frac{-i\Omega}{\gamma} \right) e^{-i\Omega\eta} + \frac{F_{-\gamma-i\Omega}(e^{-a\eta})}{\gamma + i\Omega - a} \left(\left(1 + \frac{i\Omega}{\gamma} \right) e^{i\Omega\eta} - e^{-i\Omega\eta} \right) \right] \\
&\quad - \frac{1}{4} \left[\left(\frac{i\Omega}{\gamma} + e^{-2\gamma\eta} \left(\frac{i\Omega}{\gamma} + 1 - e^{-2i\Omega\eta} \right) \right) (\psi_{\gamma+i\Omega} + \psi_{-\gamma-i\Omega}) \right. \\
&\quad \left. - \left(\frac{-i\Omega}{\gamma} + e^{-2\gamma\eta} \left(\frac{i\Omega}{\gamma} + 1 - e^{-2i\Omega\eta} \right) \right) i\pi \coth \frac{\pi}{a}(\Omega - i\gamma) \right] \} . \tag{63}
\end{aligned}$$

$$\begin{aligned}
& -\langle QQ \rangle_{v2} \\
&= \frac{-2\hbar\gamma}{\pi m_0} \operatorname{Re} \{ \Lambda_{0_{v2}} - \frac{e^{-2\gamma(\tau - \tau_0)}}{8\Omega^2} \left[(1 - \frac{i\Omega}{\gamma} - e^{2i\Omega(\tau - \tau_0)}) \cdot (i\pi + 2\log(\gamma - i\Omega) + 2\Gamma(0, -(\gamma - i\Omega)(\tau - \tau_0))) \right. \\
&\quad + (1 + \frac{i\Omega}{\gamma} - e^{-2i\Omega(\tau - \tau_0)}) \cdot (-i\pi - 2\log(\gamma + i\Omega) + 2\Gamma(0, -(\gamma + i\Omega)(\tau - \tau_0))) \left. \right] \\
&\quad - \frac{i}{8\Omega\gamma} \left[-i\pi - 2\log(\frac{\gamma + i\Omega}{\gamma - i\Omega}) + 2\Gamma(0, (\gamma + i\Omega)(\tau - \tau_0)) - 2\Gamma(0, (\gamma - i\Omega)(\tau - \tau_0)) \right] \} , \tag{64}
\end{aligned}$$

where Λ_0 and $\Lambda_{0_{v2}}$ are the terms contains those divergent part ($\Gamma(0,0)$ and $\log(0)$) as $\tau'' \rightarrow \tau$ and $\tau_0'' \rightarrow \tau_0$, and are absorbed into the renormalized constant or coefficient in the experiment. Figure 3, 4 and Figure 5 are the

numerical results for $\langle QQ \rangle_{v1}$ and $-\langle QQ \rangle_{v2}$. In the plots, the red line is the term $\langle QQ \rangle_{v1}$ and the blue line is the term $-\langle QQ \rangle_{v2}$, while the black line is the sum $\langle QQ \rangle_{v1} - \langle QQ \rangle_{v2}$. The two-point function for the vacuum fluctuations part $\langle QQ \rangle_v$ (black line) begins from a relatively high value, then oscillates and reaches to a saturated value at later time.

In figure 3, we change the proper acceleration a and keep other parameters the same. We can see that for $a = 0.1$ and $a = 0.001$, the curves for black line have the same shape but the values are slightly different. The value of two-point function $\langle QQ \rangle_v$ for $a = 0.1$ curve is just higher than the $a = 0.001$ curve for a very small number 0.00001. If we think that an uniformly accelerated detector would experience a different thermal radiance—a different temperature in the background(Unruh effect) , this different background would produce a different vacuum fluctuations for $\langle QQ \rangle_v$, thus we can see that the difference of the effect from proper acceleration for $a = 0.1$ and $a = 0.001$ UAD although is small but indeed is there.

In figure 4, we change the value of the coupling constant λ_0 or say we change the decay parameter γ . Note that $\gamma = \frac{\lambda_0^2}{8\pi m_0}$ and we use perturbations method in this computation, therefore $\lambda_0 < 1$ is the basic assumption for perturbation(λ_0 is the expansion parameter). Then the allowed region for γ is that $\gamma < 0.039$. In the past work[21], we choose $\gamma = 0.1$ which is equal to $\lambda_0 = 1.585$, this value is too big and obviously violates the basic assumption of the perturbation and makes the perturbative solutions inconsistent with the perturbation method. According to our experience, a safe choice is that the expansion parameter $\lambda_0 \approx 0.1$, this is why we choose $\lambda_0 = 0.1$ and $\lambda_0 = 0.3$ (corresponding to $\gamma = 0.000398$ and $\gamma = 0.00358$) in our numerical plots.

In figure 5, we alter the value of frequency Ω (i.e. the frequency for the internal degrees of freedom of the detector) and keep other parameters the same. We choose $\Omega = 2.3$ and $\Omega = 1.0$, the magnitude of two-point function $\langle QQ \rangle_v$ for $\Omega = 2.3$ is larger than $\Omega = 1.0$ case. Also in the same τ interval, the curve for the $\Omega = 2.3$ case has more oscillations than the curve for the $\Omega = 1.0$ case.

Similar to the calculations of the two-point function $\langle QQ \rangle$, we also compute the two-point function $\langle \dot{Q} \dot{Q} \rangle$ and the result is listed below. As is shown above, there is an extra term $-\langle \dot{Q} \dot{Q} \rangle_{v2}$ in our new result which is missing in the past result [21].

$$\begin{aligned}
& \langle \dot{Q} \dot{Q} \rangle_{v1} \\
&= \frac{2\hbar\gamma}{\pi m_0 \Omega^2} \theta(\eta) \operatorname{Re} \left\{ \left(\Lambda_1 - \ln \frac{a}{\Omega} \right) \Omega^2 + \left(\Lambda_0 - \ln \frac{a}{\Omega} \right) e^{-2\gamma\eta} (\Omega \cos \Omega\eta - \gamma \sin \Omega\eta)^2 \right. \\
&\quad + \frac{a}{2} (\gamma + i\Omega)^2 e^{-(\gamma+a)\eta} \left[\frac{F_{\gamma+i\Omega}(e^{-a\eta})}{\gamma + i\Omega + a} \left(\frac{i\Omega}{\gamma} \right) e^{-i\Omega\eta} + \frac{F_{-\gamma-i\Omega}(e^{-a\eta})}{\gamma + i\Omega - a} \left(\left(1 - \frac{i\Omega}{\gamma} \right) e^{i\Omega\eta} - e^{-i\Omega\eta} \right) \right] \\
&\quad + \frac{1}{4} (\gamma + i\Omega)^2 \left[\left(\frac{i\Omega}{\gamma} + e^{-2\gamma\eta} \left(\frac{i\Omega}{\gamma} - 1 + e^{-2i\Omega\eta} \right) \right) (\psi_{\gamma+i\Omega} + \psi_{-\gamma-i\Omega}) \right. \\
&\quad \left. \left. - \left(\frac{-i\Omega}{\gamma} + e^{-2\gamma\eta} \left(\frac{i\Omega}{\gamma} - 1 + e^{-2i\Omega\eta} \right) \right) i\pi \coth \frac{\pi}{a}(\Omega - i\gamma) \right] \right\}. \tag{65}
\end{aligned}$$

$$\begin{aligned}
& -\langle \dot{Q} \dot{Q} \rangle_{v2} \\
&= \frac{-2\hbar\gamma}{\pi m_0} \theta(\eta) \operatorname{Re} \left\{ \tilde{\Lambda}_{0_{v2}} + \frac{e^{-2\gamma(\tau-\tau_0)}}{8\Omega^2} \left[((\gamma^2 + \Omega^2)(1 - \frac{i\Omega}{\gamma}) - (\gamma - i\Omega)^2 e^{2i\Omega(\tau-\tau_0)}) \right. \right. \\
&\quad \cdot (-i\pi + 2 \log(\gamma - i\Omega)) + ((\gamma^2 + \Omega^2)(1 + \frac{i\Omega}{\gamma}) - (\gamma + i\Omega)^2 e^{-2i\Omega(\tau-\tau_0)}) \cdot (i\pi + 2 \log(\gamma + i\Omega)) \left. \right] \\
&\quad + \frac{ie^{-(\gamma+i\Omega)(\tau-\tau_0)}}{4\Omega\gamma} \left[(\gamma - i\Omega) \left(\frac{-1}{\tau - \tau_0} + e^{(\gamma-i\Omega)(\tau-\tau_0)} (\gamma - i\Omega) \Gamma(0, (\gamma - i\Omega)(\tau - \tau_0)) \right) - (\gamma + i\Omega) \right. \\
&\quad \cdot \left(\frac{-1}{\tau - \tau_0} + e^{(\gamma+i\Omega)(\tau-\tau_0)} (\gamma + i\Omega) \Gamma(0, (\gamma + i\Omega)(\tau - \tau_0)) \right) \left. \right] \\
&\quad + \frac{e^{-\gamma(\tau-\tau_0)}}{4\Omega^2} \left[((\gamma + i\Omega) e^{-i\Omega(\tau-\tau_0)} - \frac{\gamma^2 + \Omega^2}{\gamma} e^{i\Omega(\tau-\tau_0)}) ((\gamma + i\Omega) (i\pi - \Gamma(0, -(\gamma + i\Omega)(\tau - \tau_0)))) \right. \\
&\quad \cdot e^{-(\gamma+i\Omega)(\tau-\tau_0)} - \frac{1}{\tau - \tau_0}) + ((\gamma - i\Omega) e^{i\Omega(\tau-\tau_0)} - \frac{\gamma^2 + \Omega^2}{\gamma} e^{-i\Omega(\tau-\tau_0)}) \cdot (e^{(-\gamma+i\Omega)(\tau-\tau_0)} (-\gamma + i\Omega) \right. \\
&\quad \left. \left. - \frac{1}{\tau - \tau_0}) \right] \right\}.
\end{aligned}$$

$$\cdot(i\pi + \Gamma(0, (-\gamma + i\Omega)(\tau - \tau_0))) - \frac{1}{\tau - \tau_0})\Big] + \frac{i}{8\Omega\gamma} [(\gamma - i\Omega)^2(2\log(\gamma - i\Omega) + i\pi) - (\gamma + i\Omega)^2(2\log(\gamma - i\Omega) + 3i\pi)]\}, \quad (66)$$

where Λ_1 , Λ_0 and $\tilde{\Lambda}_{0,v2}$ are the terms contains those divergent parts($\Gamma(0,0)$ and $\log(0)$) as $\tau'' \rightarrow \tau$ and $\tau_0'' \rightarrow \tau_0$, and they are absorbed into the renormalized constant or coefficient in the experiment.

The above numerical results are plotted in the following figures Figure 6, 7 and Figure 8. The red line is the term $\langle \dot{Q}\dot{Q} \rangle_{v1}$, while the green line is the missing term $-\langle \dot{Q}\dot{Q} \rangle_{v2}$, and the black line is the sum of $\langle \dot{Q}\dot{Q} \rangle_{v1} - \langle \dot{Q}\dot{Q} \rangle_{v2}$.

In Figure 6 , we vary the value a and find the magnitude of $\langle \dot{Q}\dot{Q} \rangle_v$ for different a ($a = 0.1$ or $a = 0.001$) at the same time τ is unchanged. The effect of proper acceleration a is not obvious. The curve at first is arising slightly and then is decreasing and oscillating. The trend for $\langle \dot{Q}\dot{Q} \rangle_v$ is decreasing and different from $\langle QQ \rangle_v$ which is slightly increasing.

In Figure 7, we vary the decay parameter γ (that is equal to vary the coupling constant λ_0). The curve for the two-point function $\langle \dot{Q}\dot{Q} \rangle_v$ is also rising slightly in the beginning and then oscillating and decreasing to a saturated value. The difference is that the curve for $\gamma = 0.00358$ arrives to the saturated value earlier than $\gamma = 0.000398$. At the same time τ , the value of the two-point function $\langle \dot{Q}\dot{Q} \rangle_v$ for different γ is also slightly different. The reason is that a higher γ value for the two-point function curve decays to the same value faster than a lower γ curve.

In Figure 8, we alter the frequency of the internal degrees of freedom for the detector. It is obvious that the magnitude of $\langle \dot{Q}\dot{Q} \rangle_v$ changes a lot when the internal frequency Ω is altered. The trend of both curves is the same that at first it has a small rise and then decays and oscillates to a saturated value. However, a large Ω has more oscillations in its decay curve. A small Ω is less active than a big Ω . And also, a small Ω curve has a much lower saturated value than a big Ω curve.

The red lines in the plots represents the old results for the two-point functions $\langle \dot{Q}\dot{Q} \rangle_v$ which is the dotted line in Fig.2 in the old result [21]. In the old results it does not have the missing term $-\langle \dot{Q}\dot{Q} \rangle_{v2}$ (the green line). The black line is the sum $\langle \dot{Q}\dot{Q} \rangle_{v1} - \langle \dot{Q}\dot{Q} \rangle_{v2}$ and it gradually drops to a steady value at late time, this is different from the old result. The two-point functions $\langle \dot{Q}\dot{Q} \rangle_v$ in the old result increases gradually to a steady value.

Comparing the above plots for the two-point function $\langle \dot{Q}\dot{Q} \rangle_v$ with the plots for the two-point function $\langle QQ \rangle_v$, we find that the difference between $\langle QQ \rangle_v$ and $\langle \dot{Q}\dot{Q} \rangle_v$ is that the proper acceleration parameter "a" affects the trend of the oscillating curve in the early time region (whether it is slightly increasing or decreasing). The coupling constant λ_0 affects how soon the curve of $\langle \dot{Q}\dot{Q} \rangle$ arrives at the saturated value as shown in Figure 7. The frequency Ω affects how large the final saturated value for $\langle \dot{Q}\dot{Q} \rangle$ will be as shown in Figure 8, a smaller Ω has a smaller saturated value.

Next, we will discuss the allowed region for the value of the coupling constant λ_0 , which is about the decay constant γ and this part is not noticed before.

5. Allowed region for γ : proper and improper value for γ —about the contribution of the missing term $-\langle QQ \rangle_{v2}$

The γ value has some restrictions. In Sec.II and the previous part of this Section, we expand the mode function $f^{(\pm)}$ and $q^{(\pm)}$ by the order of λ_0 , and then use the perturbative method to obtain the leading order solutions for $q^{(\pm)}$. Later, we use the leading order solution to compute $\langle Q^2(\eta) \rangle_v$ to the first order $O(\lambda_0)$. Thus, λ_0 is the expansion parameter and it is supposed to be smaller than 1. While the decay parameter γ is defined as $\gamma = \frac{\lambda_0^2}{8\pi m_0}$, therefore the value of γ has an allowed region which is corresponding to $\lambda_0 < 1$.

In the past work [21], we took $\gamma = 0.1$, this value is corresponding to $\lambda_0 \approx 1.58$, and it apparently is larger than 1. In such case, the perturbative solution is no longer consistent with our assumption(i.e. λ_0 is smaller than 1) if we take $\gamma = 0.1$. Let us see what will happen if we take $\gamma = 0.1$ in the numerical calculations.

In Figure 9, we do the numerical calculations for two cases that $\gamma = 0.1$ (i.e. equal to $\lambda_0 \approx 1.58$) and $\gamma = 0.000398$ (i.e. equal to $\lambda_0 = 0.1$) with other parameters $\Omega = 2.3$ and $a = 0.001$ are fixed. In the $\gamma = 0.1$ plot, the missing term (blue line) $\langle Q^2(\eta) \rangle_{v2}$ becomes unimportant very soon, it drops quickly and then the total effect(black line) is dominated by the red line $\langle Q^2(\eta) \rangle_{v1}$. The trend of the black line is similar to the red line, both lines are increasing. If

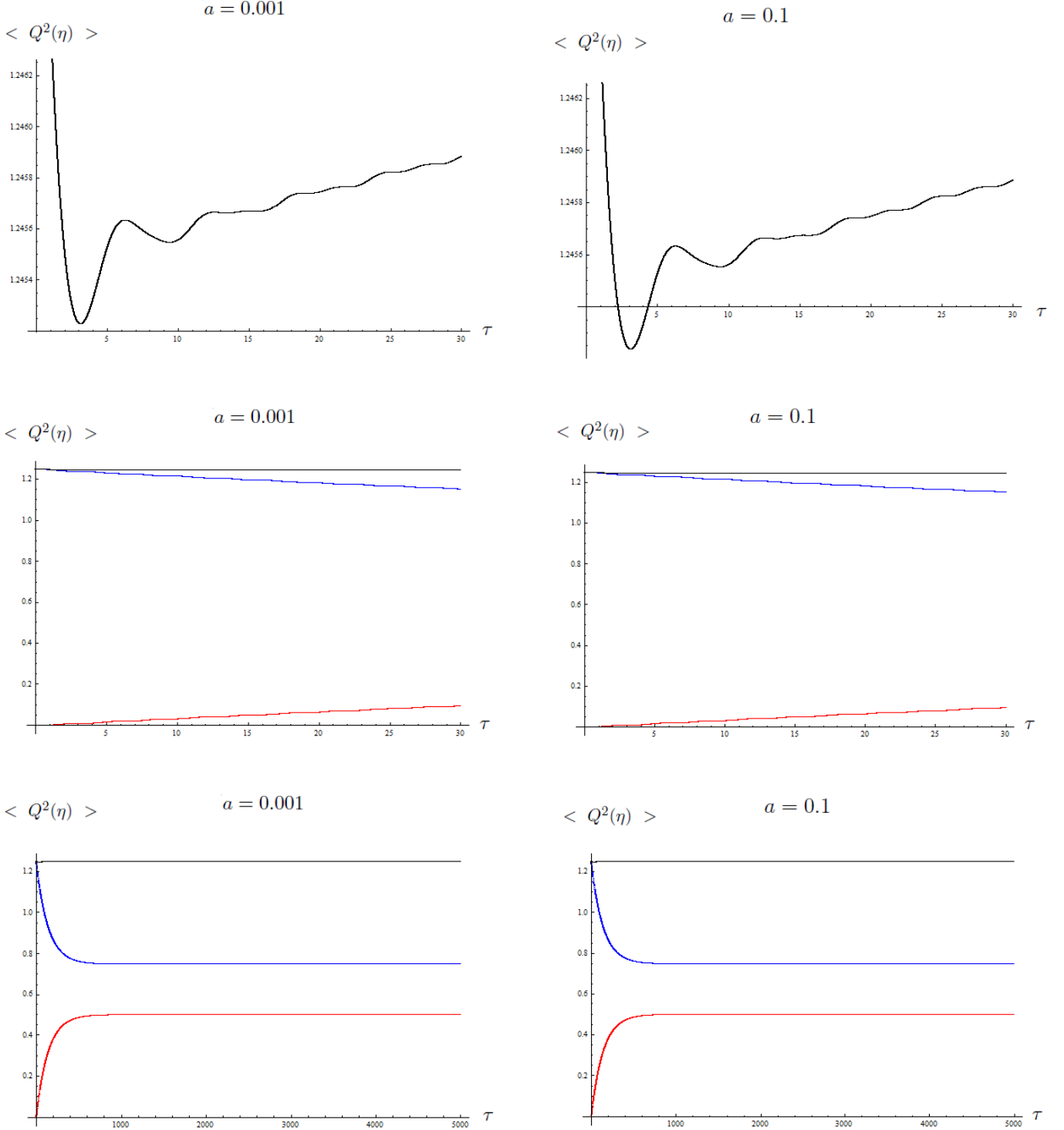


FIG. 3: The plots for $\langle Q^2(\eta) \rangle_{v1}$ (red line, Eq.(63) with Λ_0 excluded), and $-\langle Q^2(\eta) \rangle_{v2}$ (blue line, Eq.(64) with $\Lambda_0 v_2$ excluded), and the total $\langle Q^2(\eta) \rangle_v$ (i.e. black line $\langle Q^2(\eta) \rangle_{v1} - \langle Q^2(\eta) \rangle_{v2}$). Here $\Omega = 1.0$, $\lambda_0 = 0.3$ (which is $\gamma = 0.00358$) and $m_0 = \hbar = 1$. Note that $-\langle Q^2(\eta) \rangle_{v2}$ is bigger than $\langle Q^2(\eta) \rangle_{v1}$. The black line (i.e. $\langle Q^2(\eta) \rangle_v$) oscillates in the beginning and then arrives at the saturated value later. When $t = 30$, the curve for the proper acceleration $a = 0.1$ arrives at the value 1.24589 while the curve for a smaller proper acceleration $a = 0.001$ arrives at the value 1.24588, the difference is only 0.00001. When $t = 5000$, both curves for small or large proper acceleration value arrive at the same final magnitude 1.24772.

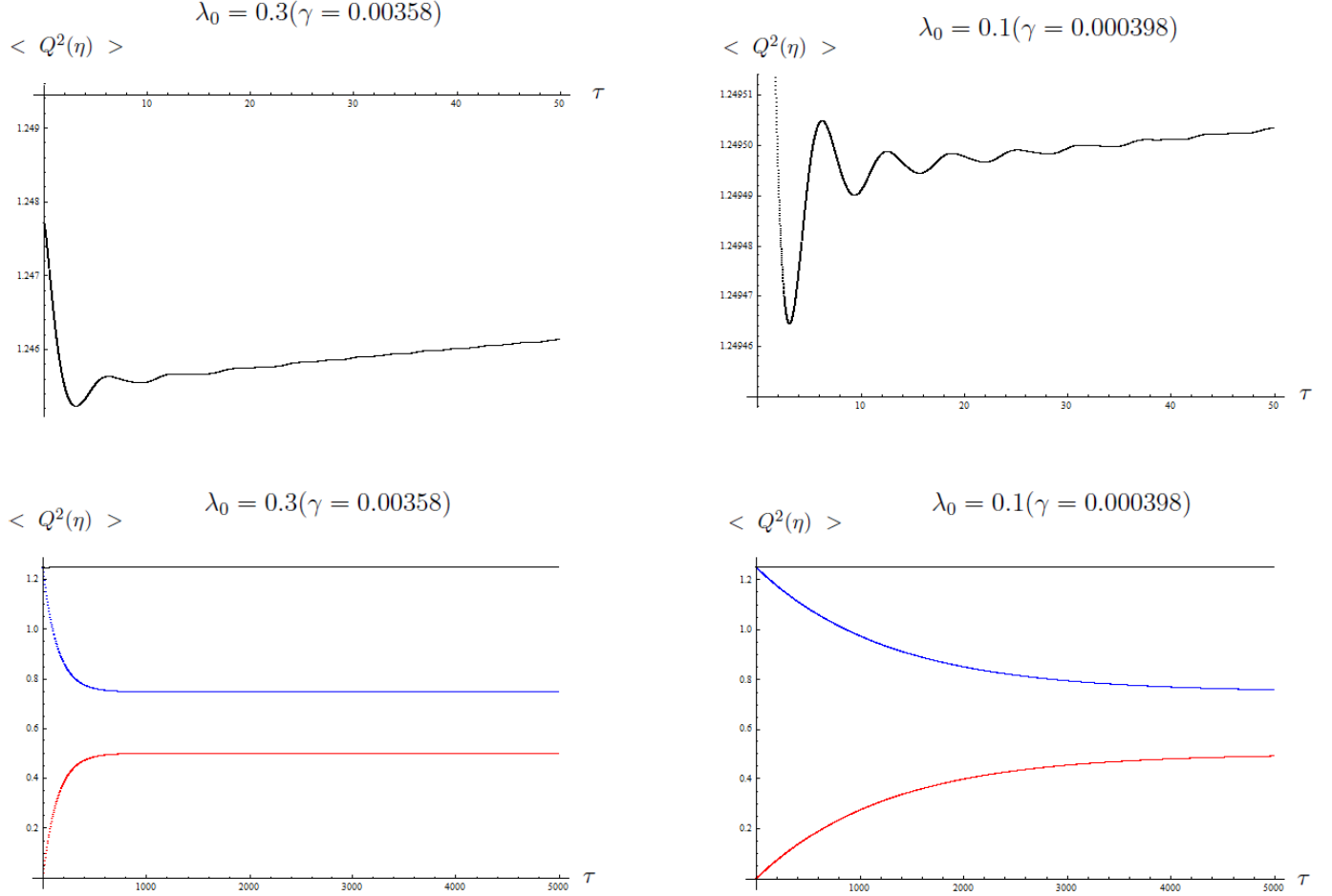


FIG. 4: The decay parameter $\gamma(\gamma = \frac{\lambda_0^2}{8\pi m_0})$. The plots for $\langle Q^2(\eta) \rangle_{v1}$ (red line, Eq.(63) with Λ_0 excluded), and $-\langle Q^2(\eta) \rangle_{v2}$ (blue line, Eq.(64) with Λ_0_{v2} excluded), and the total $\langle Q^2(\eta) \rangle_v$ (black line $\langle Q^2(\eta) \rangle_{v1} - \langle Q^2(\eta) \rangle_{v2}$). Here $\Omega = 1.0$, $a = 0.001$ and $m_0 = \hbar = 1$. The decay parameter is different in the plots. The black lines oscillate in the beginning and then arrives at different saturated values later at proper time $\tau = 5000$ for different λ_0 . When $\tau = 50$, the final value for $\gamma = 0.000398$ is 1.2495, while when $\tau = 50$, the final value for $\gamma = 0.00358$ is 1.24613. When $\tau = 5000$, the final value for $\gamma = 0.000398$ is 1.24974, while when $\tau = 5000$, the final value for $\gamma = 0.00358$ is 1.24772. A large $\lambda_0(\lambda_0 = 0.3)$ has a larger value than a smaller $\lambda_0(\lambda_0 = 0.1)$, while a smaller λ_0 arrives at the same saturated value later than a larger $\lambda_0(\lambda_0 = 0.3)$. The decay parameter γ affects the saturated time.

we lost the second term $\langle Q^2(\eta) \rangle_{v2}$ in our analytic calculations and then we would like to do the numerical integrations in the very beginning as a double check, in order to get a consistent result(means the trend of black line and red line are similar and have the same trend, because the numerical calculation doesn't forget the missing term so that it will give us the black line), one must choose a particular value for the parameter γ which is $\gamma = 0.1$ (i.e. $\lambda_0 \approx 1.58$). For $\gamma = 0.1$, the numerical result (black line) will show the same trend as the red line(because the second term $-\langle Q^2(\eta) \rangle_{v2}$ is unimportant under such γ value). In short words, we must pick up a value for γ such that it would make the blue line value small and unimportant. The value $\gamma = 0.1$ fits this goal. And, we would thought that our analytic results were correct because both analytic and numerical calculations gave us the similar curves for the two-point function $\langle Q^2(\eta) \rangle_v$. However, this is just an improper γ value gives us a misleading. Thus, we must be careful about the allowed and not allowed region for the parameters in the solutions when we do the numerical calculations as a double check.

If one drops the missing term and chooses an allowed γ value as is shown in Figure 3 and Figure 4 (i.e. $\gamma = 0.000398$), the trend of the black line and the red line looks different—the red line is increasing (with some ripples on it) but the black line looks quite flat. Without notice the missing term, one may give up this value for γ and go back to

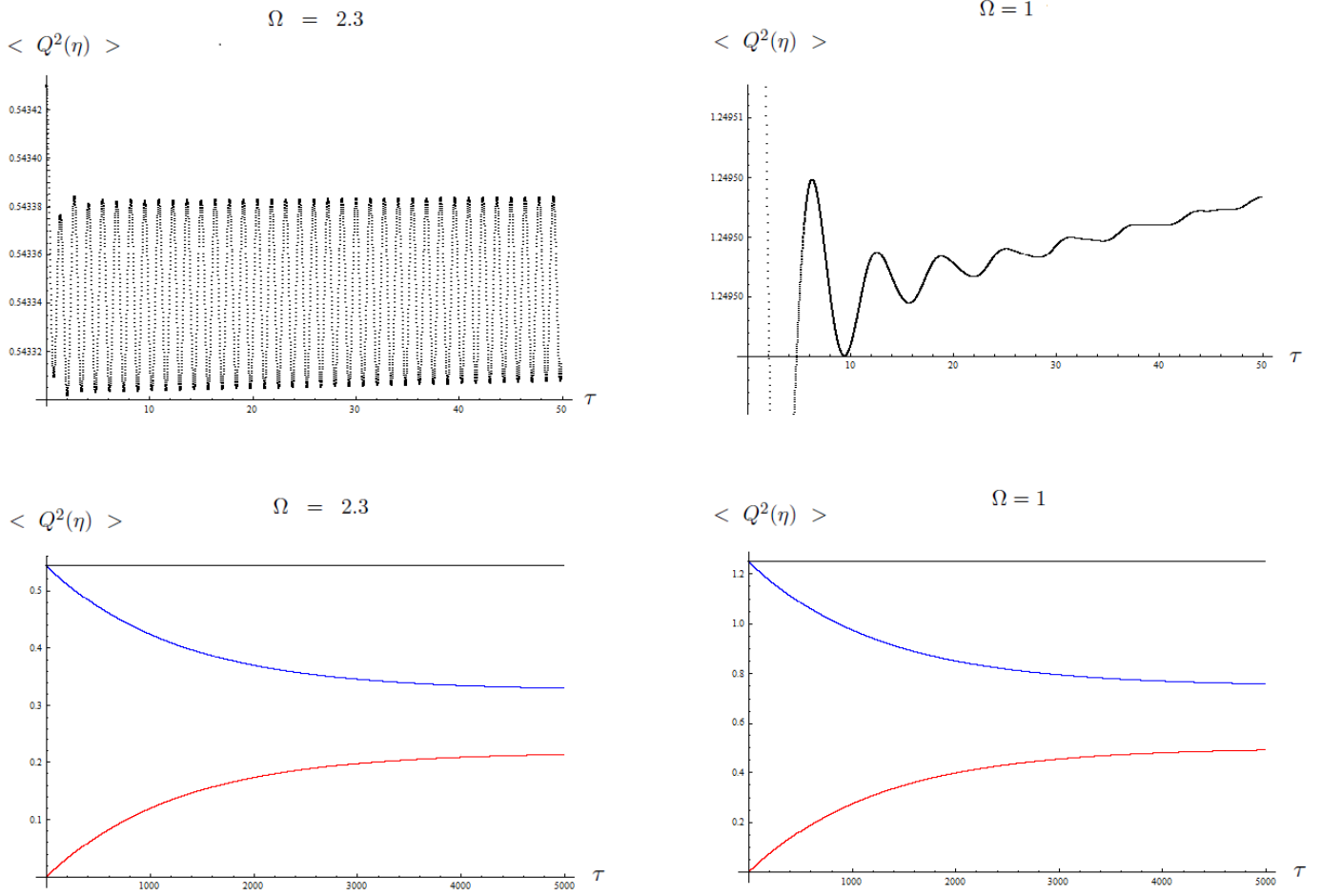


FIG. 5: The frequency Ω . The plot for $\langle Q^2(\eta) \rangle_{v1}$ (red line, Eq.(63) with Λ_0 excluded), and $-\langle Q^2(\eta) \rangle_{v2}$ (blue line, Eq.(64) with Λ_{0v2} excluded), and the total $\langle Q^2(\eta) \rangle_v$ (black line, which is $\langle Q^2(\eta) \rangle_{v1} - \langle Q^2(\eta) \rangle_{v2}$). Here $a = 0.001$, $\lambda_0 = 0.1$ ($\gamma = 0.000398$) and $m_0 = \hbar = 1$. Two values of Ω are chosen ($\Omega = 2.3$ and $\Omega = 1.0$). The curves arrive at different saturated value for different Ω . The smaller Ω ($\Omega = 1.0$) has a higher saturated value than the bigger Ω ($\Omega = 2.3$) at later time $\tau = 5000$. When $\tau = 5000$, the final value for $\Omega = 2.3$ is $\langle Q^2(\eta) \rangle_v = 0.543429$, while the final value for $\Omega = 1.0$ is $\langle Q^2(\eta) \rangle_v = 1.24974$. The frequency parameter Ω affects the final saturated value. Also, a bigger Ω has more vibrations in the same τ region and is more active.

the not allowed value $\gamma = 0.1$ and think that the numerical test is consistent with ones analytic result (drop the missing term). This case may give one a misleading double check that ones analytic and numerical computations are consistent in that γ value ($\gamma = 0.1$), so ones analytic results are correct. But in fact the contribution of the missing term is suppressed in a not allowed γ region.

Besides, one thing is important that we should be careful when we choose the value of a . If we set the light speed $c = 1$, then the proper acceleration a is smaller than 1 (i.e. $a < 1$). In our present numerical calculations, we choose the proper acceleration $a = 0.1$ or $a = 0.001$ both are smaller than 1. In the past work, we choose $a = 1$ and this value is not a good choice if we assume the light speed $c = 1$. The value $a = 1$ is too big.

Next, we will continue to consider the inertial detector case.

6. Trajectory 2 : Inertial detector

Now, we will calculate the two-point correlation functions $\langle Q^2(\eta) \rangle_v$ and $\langle \dot{Q}^2(\eta) \rangle_{v2}$ for inertial detector Bob along the trajectory $\tilde{z}_B^\mu = (\gamma\tau, \gamma v\tau + x_a + d, 0, 0)$. This trajectory is for an observer moves at constant velocity and has

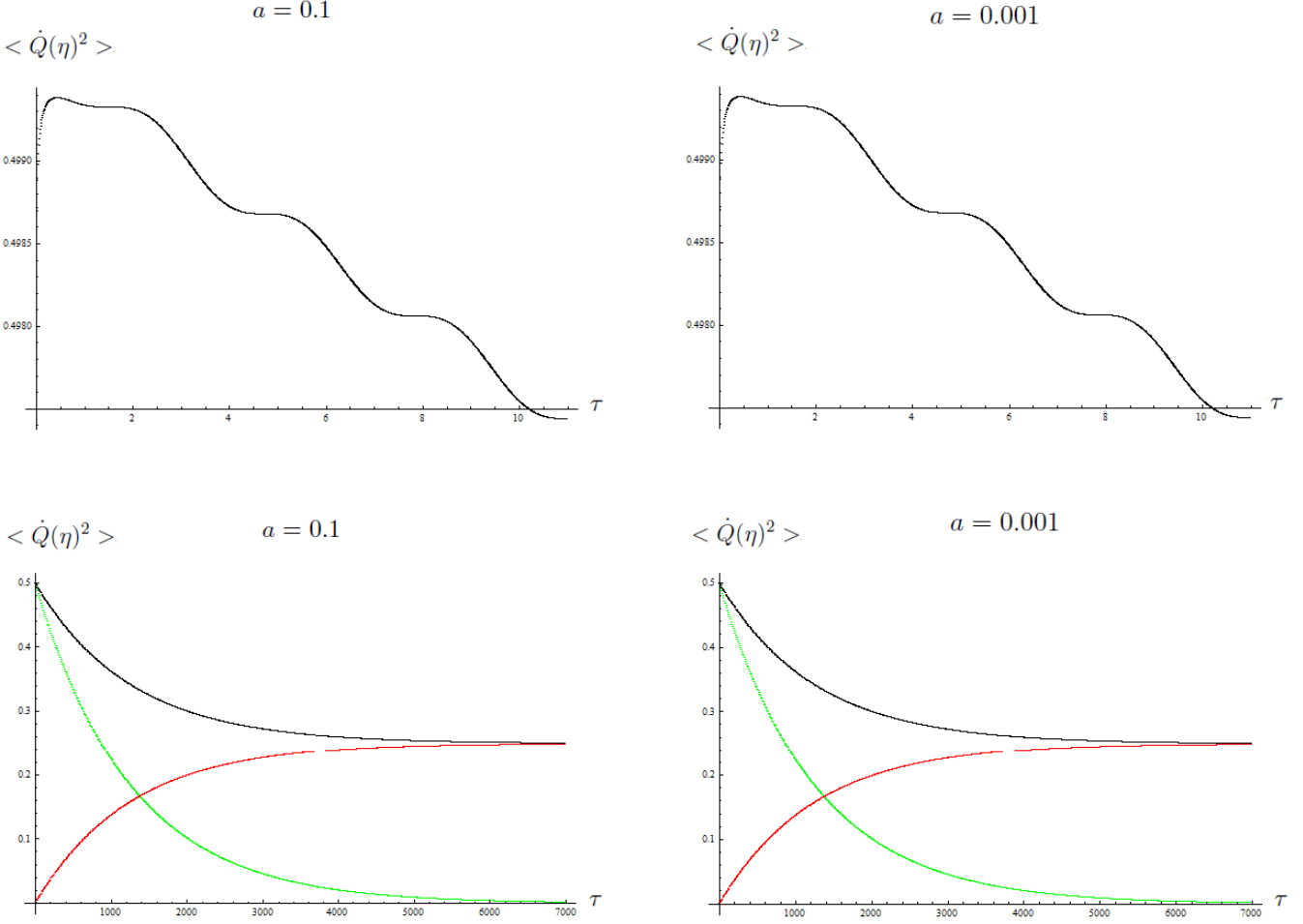


FIG. 6: The proper acceleration a . The plots for $\langle \dot{Q}^2(\eta) \rangle_{v1}$ (red line, Eq.(65) with Λ_1 excluded), and $-\langle \dot{Q}^2(\eta) \rangle_{v2}$ (green line, Eq.(66) with $\tilde{\Lambda}_{0v2}$ excluded), and the total $\langle \dot{Q}^2(\eta) \rangle_v$ (black line, which is $\langle \dot{Q}^2(\eta) \rangle_{v1} - \langle \dot{Q}^2(\eta) \rangle_{v2}$). Here $\Omega = 1.0$, $\lambda_0 = 0.1$ (which is $\gamma = 0.000398$) and $m_0 = \hbar = 1$. The green line $-\langle \dot{Q}^2(\eta) \rangle_{v2}$ is bigger than $\langle \dot{Q}^2(\eta) \rangle_{v1}$ in the early time region. The black line oscillates in the beginning and then arrives at the saturated value later around $\tau \approx 6500$. For $\tau = 11$ both $a = 0.1$ and $a = 0.001$ curves arrive at the same value $\langle \dot{Q}^2(\eta) \rangle_v = 0.497442$, when $\tau = 7000$ both $a = 0.1$ and $a = 0.001$ curves arrive at the same value $\langle \dot{Q}^2(\eta) \rangle_v = 0.250765$. For $\langle \dot{Q}^2(\eta) \rangle_v$, the difference between the proper acceleration $a = 0.1$ and $a = 0.001$ is not obvious as shown in the plots. However, the trend of the curve for the two-point function $\langle \dot{Q}^2(\eta) \rangle_v$ is decreasing, and is different from the $\langle Q^2(\eta) \rangle_v$ plots.

a finite distance d away from the other static detector Alice. This part is different from the one in the past work that one apply the UAD result and take the limit $a \rightarrow 0$ to be the result for an inertial detector. In the previous subsections, we already know that in such limit $a \rightarrow 0$ the UAD Bob is shifted to very far away and can not exchange the signal with Alice in a reasonable time interval.

To get the two-point correlation functions for the inertial detector Bob, we just need to plug the inertial trajectory $\tilde{z}_B^\mu = (\gamma\tau, \gamma v\tau + x_a + d, 0, 0)$ into Eq.(46), then the difference is that z^0 and \vec{z} in F are changed. The integral F for this new \tilde{z}_B^μ is the following

$$F = \frac{\hbar}{(2\pi)^3} \int_0^{2\pi} d\phi \int_{-1}^1 d(\cos\theta) \int_0^\infty \frac{\omega^2 d\omega}{2\omega} \int_{-\infty}^\infty \frac{dt}{2\pi} \int_{-\infty}^\infty \frac{dt'}{2\pi} e^{i\kappa t - i\kappa' t' - i\omega(z^0(t) - z^0(t') + i\omega \cos\theta |\vec{z} - \vec{z}'|)}$$

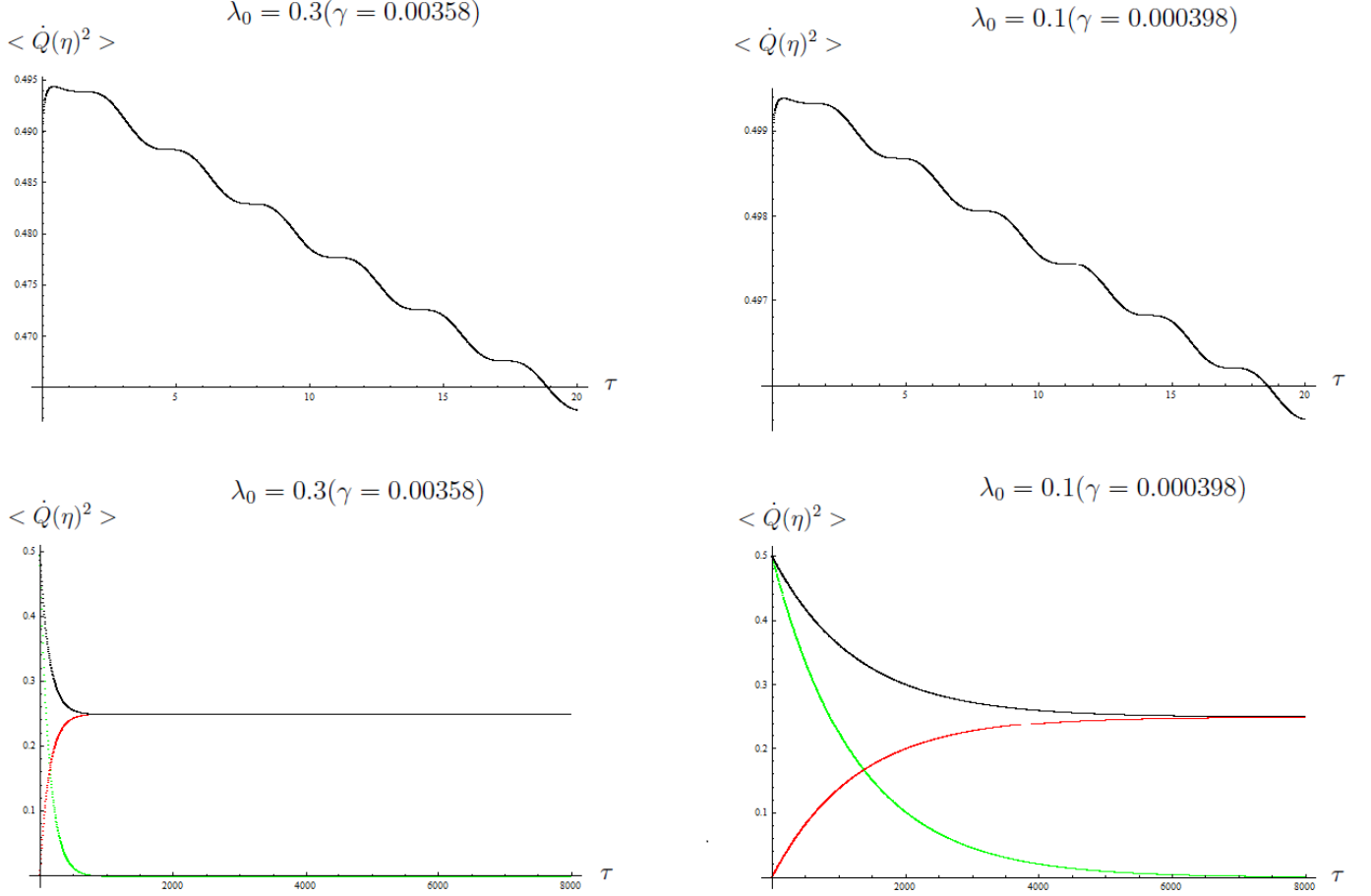


FIG. 7: The decay parameter γ (i.e. the coupling constant λ_0). The plots for $\langle \dot{Q}^2(\eta) \rangle_{v1}$ (red line, Eq.(65) with Λ_1 excluded), and $-\langle \dot{Q}^2(\eta) \rangle_{v2}$ (green line, Eq.(66) with $\tilde{\Lambda}_{0v2}$ excluded), and the total $\langle \dot{Q}^2(\eta) \rangle_v$ (black line, which is $\langle \dot{Q}^2(\eta) \rangle_{v1} - \langle \dot{Q}^2(\eta) \rangle_{v2}$). Here $\Omega = 1.0$, $a = 0.1$ and $m_0 = \hbar = 1$. The coupling constant λ_0 is different in these plots. When $\tau = 20$, $\langle \dot{Q}^2(\eta) \rangle_v = 0.4956$ for $\gamma = 0.000398$ and $\langle \dot{Q}^2(\eta) \rangle_v = 0.462788$ for $\gamma = 0.00358$. At late time when $\tau = 8000$, $\langle \dot{Q}^2(\eta) \rangle_v = 0.250238$ for $\gamma = 0.000398$ and $\langle \dot{Q}^2(\eta) \rangle_v = 0.248185$ for $\gamma = 0.00358$. A larger γ has a higher $\langle \dot{Q}^2(\eta) \rangle_v$ value than a smaller decay parameter γ . The lines are oscillating in the early time region and then arrive at a saturated value at late time. A bigger γ decays faster than a smaller γ , and the trend of $\langle \dot{Q}^2(\eta) \rangle_v$ curve is decreasing except a very short-time small rise in the beginning.

$$\begin{aligned}
&= \frac{\hbar}{2\pi} \int_0^\infty d\omega \int_{-\infty}^\infty \frac{dt}{2\pi} \int_{-\infty}^\infty \frac{dt'}{2\pi} e^{i\kappa t - i\kappa' t' - i\omega[z^0(t) - z^0(t')]} \frac{\sin(\omega|\vec{z}(t) - \vec{z}(t')|)}{|\vec{z}(t) - \vec{z}(t')|} \\
&= \frac{\hbar}{(2\pi)^4} \int_{-\infty}^\infty dt \int_{-\infty}^\infty dt' \frac{e^{i\kappa(t - \frac{i\epsilon}{2}) - i\kappa'(t' + \frac{i\epsilon}{2})}}{|\vec{z}(t - \frac{i\epsilon}{2}) - \vec{z}(t' + \frac{i\epsilon}{2})|^2 - [z^0(t - \frac{i\epsilon}{2}) - z^0(t + \frac{i\epsilon}{2})]^2} \\
&= \frac{\hbar}{(2\pi)^4} \int_{-\infty}^\infty dt \int_{-\infty}^\infty dt' \frac{e^{\frac{\epsilon}{2}(\kappa + \kappa') + i\kappa t - i\kappa' t'}}{\gamma^2(\tau - \tau' - i\epsilon)^2(v^2 - 1)} \\
&= \frac{\hbar}{(2\pi)^4} \int_{-\infty}^\infty dT \int_{-\infty}^\infty d\Delta \frac{e^{\frac{\epsilon}{2}(\kappa + \kappa') + i(\kappa - \kappa')T + \frac{i\Delta}{2}(\kappa + \kappa')}}{-(\Delta - i\epsilon)^2} \\
&= \frac{\hbar}{(2\pi)^3} \delta(\kappa - \kappa') \int_{-\infty}^\infty d\Delta \frac{e^{\kappa\epsilon} e^{i\kappa\Delta}}{-(\Delta - i\epsilon)^2} \\
&= \frac{\hbar}{(2\pi)^2} \delta(\kappa - \kappa') \kappa, \quad \kappa \geq 0,
\end{aligned} \tag{67}$$

note that $F = 0$ when $\kappa < 0$. The velocity v is canceled in the denominator and not appear in the integration term

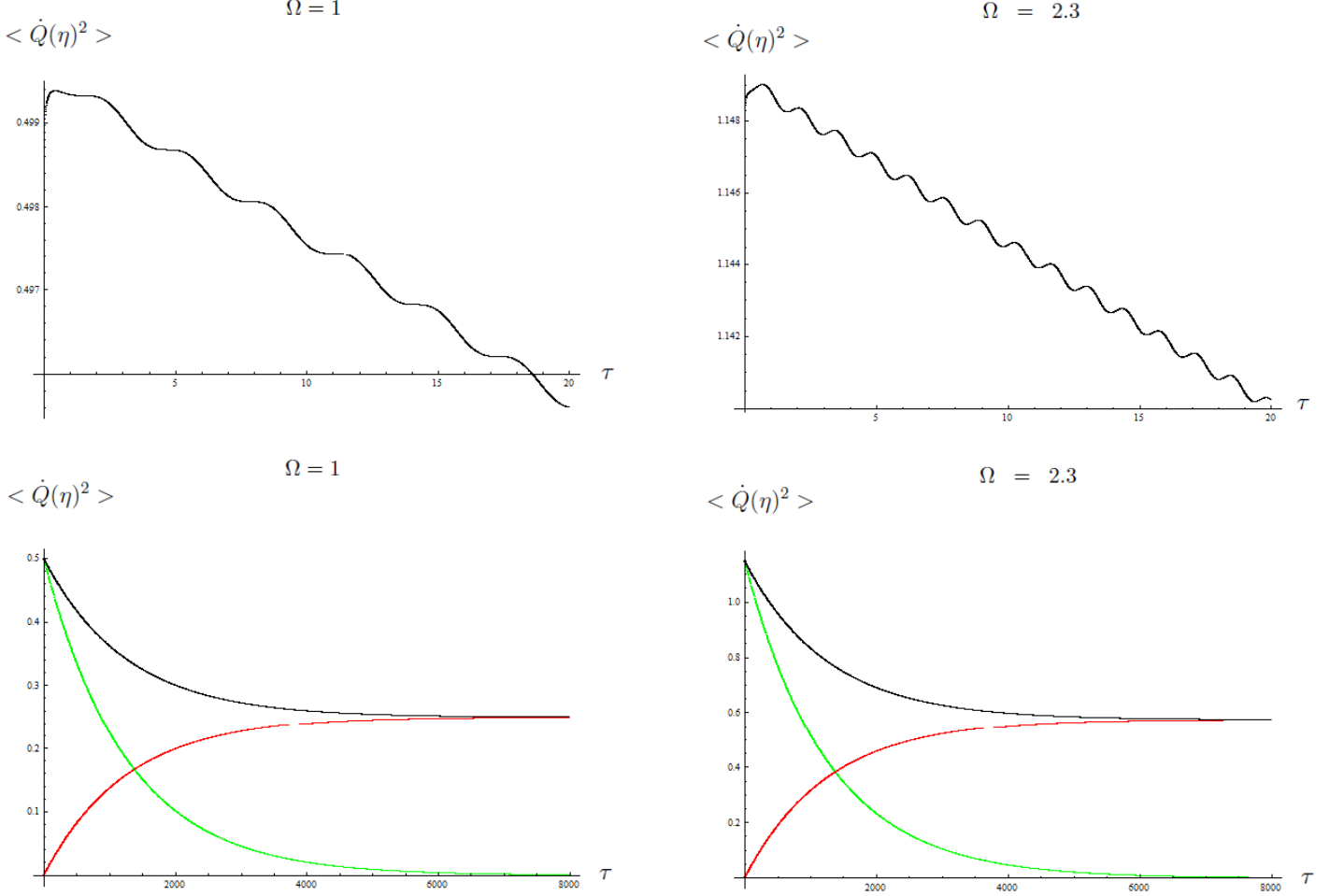


FIG. 8: The frequency parameter Ω . The plots for $\langle Q^2(\eta) \rangle_{v1}$ (red line, Eq.(65) with Λ_1 excluded), and $-\langle Q^2(\eta) \rangle_{v2}$ (green line, Eq.(66) with $\tilde{\Lambda}_{0v2}$ excluded), and the total $\langle Q^2(\eta) \rangle_v$ (black line, which is $\langle Q^2(\eta) \rangle_{v1} - \langle Q^2(\eta) \rangle_{v2}$). Here $a = 0.1$, $\gamma = 0.000398$ ($\lambda_0 = 0.1$) and $m_0 = \hbar = 1$. A larger Ω has a higher value for the two-point function $\langle Q^2(\eta) \rangle_v$. The black line has a small rise in the beginning and then decreases to a saturated value. A larger Ω has more oscillations in a same time interval than a smaller Ω . The magnitude of Ω alters the intensity of the two-point function $\langle Q^2(\eta) \rangle_v$.

F , which implies that no matter how fast or slow the velocity is, the result for F is the same.

Similar to Eq.(50), plugging F back to the two point function $\langle Q(\tau - \tau_0)Q(\tau'' - \tau_0'') \rangle_v$ and performing the integration of τ , we have the two-point function for the inertial detector

$$\begin{aligned}
 & \langle Q(\tau - \tau_0)Q(\tau'' - \tau_0'') \rangle_v \\
 &= \frac{\lambda_0^2 \hbar}{(2\pi)^2 m_0^2} \sum_{j,j'} \int_0^\infty \kappa d\kappa \frac{c_j c_{j'}^* e^{-i\kappa(\tau_0 - \tau_0'')}}{(w_j + i\kappa)(w_{j'}^* - i\kappa)} (e^{w_j(\tau - \tau_0)} - e^{-i\kappa(\tau - \tau_0)}) \\
 & \quad \cdot (e^{w_{j'}^*(\tau'' - \tau_0'')} - e^{-i\kappa(\tau'' - \tau_0'')}). \tag{68}
 \end{aligned}$$

Performing the κ integration, and then using the same calculation steps for the uniformly accelerated detector in the previous subsections, we obtain the following result for the two-point correlation function of the inertial detector Bob

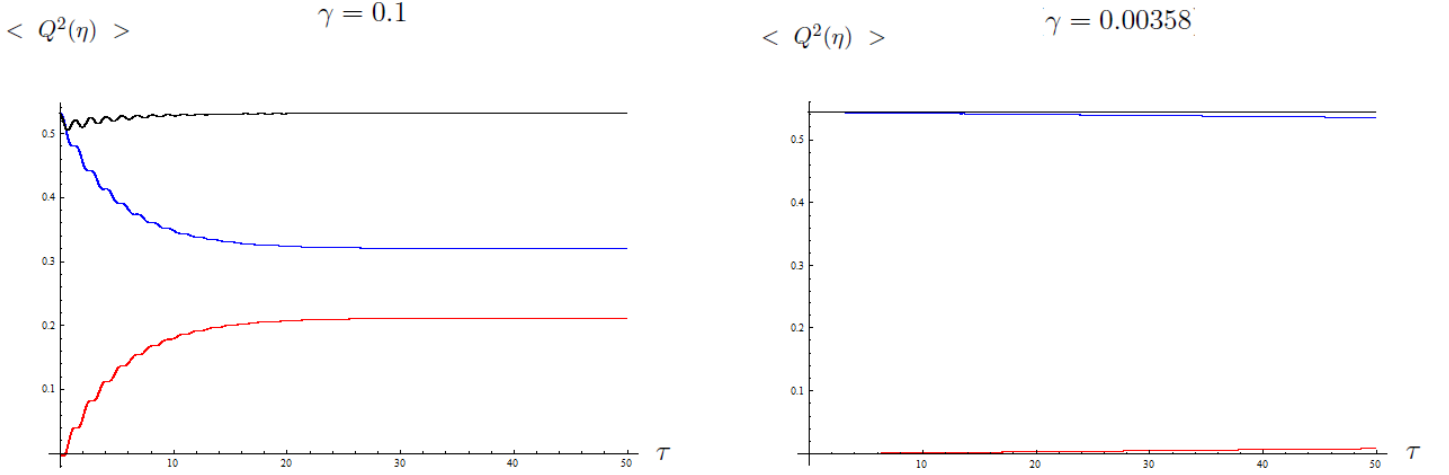


FIG. 9: The frequency parameter Ω . The plots for $\langle Q^2(\eta) \rangle_{v1}$ (red line, Eq.(65) with Λ_1 excluded), and $-\langle Q^2(\eta) \rangle_{v2}$ (green line, Eq.(66) with $\tilde{\Lambda}_{0v2}$ excluded), and the total $\langle Q^2(\eta) \rangle_v$ (black line, which is $\langle Q^2(\eta) \rangle_{v1} - \langle Q^2(\eta) \rangle_{v2}$). Here $a = 0.1$, $\gamma = 0.000398$ ($\lambda_0 = 0.1$) and $m_0 = \hbar = 1$. A larger Ω has a higher value for the two-point function $\langle Q^2(\eta) \rangle_v$. The black line has a small rise in the beginning and then is decreasing to a saturated value. A larger Ω has more oscillations in the same time interval than a smaller Ω . The magnitude of Ω alters the intensity of the two-point function $\langle Q^2(\eta) \rangle_v$.

$$\begin{aligned}
 \langle Q(\eta)^2 \rangle_v &\equiv \lim_{\eta'' \rightarrow \eta} \frac{1}{2} \langle \{Q(\eta), Q(\eta'')\} \rangle_v \\
 &= \frac{2\hbar\gamma}{\pi m_0} \theta(\eta) \text{Re}\{\tilde{\Lambda}_0 + \frac{e^{-2\gamma(\tau-\tau_0)}}{8\Omega^2} \left[(1 - \frac{i\Omega}{\gamma} - e^{2i\Omega(\tau-\tau_0)})(i\pi - 2\log(\gamma - i\Omega) + \Gamma(0, (-\gamma + i\Omega)(\tau - \tau_0))) \right. \\
 &\quad \left. + (1 + \frac{i\Omega}{\gamma} - e^{-2i\Omega(\tau-\tau_0)})(-3i\pi - 2\log(\gamma + i\Omega) + \Gamma(0, -(\gamma + i\Omega)(\tau - \tau_0))) \right] + \frac{i}{8\Omega\gamma} \\
 &\quad \cdot [-2i\pi + 2\log(\gamma - i\Omega) - 2\log(\gamma + i\Omega) - \Gamma(0, (\gamma - i\Omega)(\tau - \tau_0)) + \Gamma(0, (\gamma + i\Omega)(\tau - \tau_0))] \} . \tag{69}
 \end{aligned}$$

where $\tilde{\Lambda}_0$ contains those divergent parts ($\Gamma(0, 0)$ and $\log(0)$) as $\tau'' \rightarrow \tau$ and $\tau''_0 \rightarrow \tau_0$ and are absorbed into the renormalized constant or coefficient in the experiment.

Similarly, the result of $\langle \dot{Q}(\eta)^2 \rangle$ is written down in the following

$$\begin{aligned}
 \langle \dot{Q}(\eta)^2 \rangle_v &\equiv \lim_{\eta'' \rightarrow \eta} \frac{1}{2} \langle \{Q(\eta), Q(\eta'')\} \rangle_v \\
 &= \frac{2\hbar\gamma}{\pi m_0} \theta(\eta) \text{Re}\{\tilde{\Lambda}_{0v} + \frac{e^{-2\gamma(\tau-\tau_0)}}{8\Omega^2} \left[\left(\frac{(\gamma - i\Omega)(\gamma^2 + \Omega^2)}{\gamma} - (\gamma - i\Omega)^2 e^{2i\Omega(\tau-\tau_0)} \right) (-i\pi - 2\log(\gamma - i\Omega)) \right. \\
 &\quad \left. + \left(\frac{(\gamma + i\Omega)(\gamma^2 + \Omega^2)}{\gamma} - (\gamma + i\Omega)^2 e^{-2i\Omega(\tau-\tau_0)} \right) (-i3\pi - 2\log(\gamma + i\Omega)) \right] \\
 &\quad + \frac{e^{(-\gamma+i\Omega)(\tau-\tau_0)}}{8\Omega^2} \left[\gamma - i\Omega - \frac{(\gamma - i\Omega)^2}{\gamma} \right] \left[\frac{2}{\tau - \tau_0} - 2(\gamma - i\Omega) e^{(\gamma - i\Omega)(\tau - \tau_0)} \Gamma(0, (\gamma - i\Omega)(\tau - \tau_0)) \right] \\
 &\quad + \frac{e^{(-\gamma-i\Omega)(\tau-\tau_0)}}{8\Omega^2} \left[\gamma + i\Omega - \frac{(\gamma + i\Omega)^2}{\gamma} \right] \left[\frac{2}{\tau - \tau_0} - 2(\gamma + i\Omega) e^{(\gamma + i\Omega)(\tau - \tau_0)} \Gamma(0, (\gamma + i\Omega)(\tau - \tau_0)) \right] \\
 &\quad + \frac{e^{-\gamma(\tau-\tau_0)}}{8\Omega^2} \left[(-2i \sin(\Omega(\tau - \tau_0)) + \frac{i\Omega}{\gamma} e^{i\Omega(\tau - \tau_0)}) \left[\frac{2(\gamma + i\Omega)}{\tau - \tau_0} - 2(\gamma + i\Omega)^2 e^{-(\gamma + i\Omega)(\tau - \tau_0)} (i\pi \right. \right. \\
 &\quad \left. \left. - \Gamma(0, -(\gamma + i\Omega)(\tau - \tau_0))) \right] + (2i \sin(\Omega(\tau - \tau_0)) - \frac{i\Omega}{\gamma} e^{-i\Omega(\tau - \tau_0)}) \left[\frac{2(\gamma - i\Omega)}{\tau - \tau_0} \right. \right. \\
 &\quad \left. \left. - 2(\gamma - i\Omega)^2 e^{-(\gamma - i\Omega)(\tau - \tau_0)} (i\pi - \Gamma(0, (\gamma - i\Omega)(\tau - \tau_0))) \right] \right] \} . \tag{70}
 \end{aligned}$$

$$+2(\gamma - i\Omega)^2 e^{-(\gamma - i\Omega)(\tau - \tau_0)} \cdot (i\pi + \Gamma(0, -(\gamma - i\Omega)(\tau - \tau_0))) \Big] \Big] + \frac{i}{8\Omega\gamma} \cdot \\ [-(\gamma - i\Omega)^2 (2\log(\gamma - i\Omega) - i\pi) + (\gamma + i\Omega)^2 (2\log(\gamma + i\Omega) + i\pi) \} , \quad (70)$$

where $\tilde{\Lambda}_{0v}$ contains those divergent parts($\Gamma(0,0)$ and $\log(0)$) as $\tau'' \rightarrow \tau$ and $\tau_0'' \rightarrow \tau_0$ and are absorbed into the renormalized constant or coefficient in the experiment.

Note that the condition $\kappa \geq 0$ is very important in Eq.(67). If one does not notice that $\kappa \geq 0$ and take the integration region of κ from $-\infty$ to ∞ in Eq.(68)(i.e. $\int_{-\infty}^{+\infty} \kappa d\kappa f(\kappa)$), then one will have $\langle Q(\eta)^2 \rangle_v = 0$ in Eq.(69) for the inertial detector. This implies that the variance from the quantum field is zero and it is highly unlikely because a quantum field always contributes a nonzero variance. Actually, this strange result is the motivation for us that made us to recheck the two-point function $\langle Q(\eta)^2 \rangle_v$ for the UAD and inertial detectors. An interesting point is that Eq.(68) can be reshaped as the form in Eq.(62)(i.e. $\int_0^{+\infty} \kappa d\kappa f(\kappa) = \int_{-\infty}^{+\infty} \kappa d\kappa f(\kappa) - \int_{-\infty}^0 \kappa d\kappa f(\kappa)$), thus the two-point function $\langle Q(\eta)^2 \rangle_v$ is nonzero and the variance for the inertial detector is nonzero if we insist to take the integration region of κ is that $\int_{-\infty}^{+\infty} \kappa d\kappa f(\kappa)$ (i.e. this integration region is what we applied in the past calculations). Therefore we think that the second term $\langle Q(\eta)^2 \rangle_{v2}$ is the missing term and is important when we talk about the variance from the quantum field for the inertial detector. The missing term also changes the trend for the two-point function $\langle \dot{Q}(\eta)^2 \rangle_v$ curve in the UAD case as shown in the earlier subsection. Later, we will plot the curves of the two-point functions $\langle Q(\eta)^2 \rangle_v$ and $\langle \dot{Q}(\eta)^2 \rangle_v$ for the inertial detector.

The numerical plots for $\langle Q(\eta)^2 \rangle_v$ and $\langle \dot{Q}(\eta)^2 \rangle_v$ are shown in Figure 10 and Figure 11. The values for the two-point functions $\langle Q(\eta)^2 \rangle_v$ and $\langle \dot{Q}(\eta)^2 \rangle_v$ have the same trend. At first, the values increase slowly with ripples on the curve, and then reaches a saturated value. This is different from the UAD case, for example in Figure 3, the amplitude of the ripples gradually becomes small. For the UAD case, the early amplitude is larger than the later amplitudes. Note that the value for the two-point correlation functions of UAD changes just a little comparing to the inertial detector , the curve for UAD is quite flat. The magnitude of $\langle Q(\eta)^2 \rangle_v$ for the inertial detector has an obvious change from the beginning to the end. Besides, the ripples on the inertial detector curve of the two-point function $\langle Q(\eta)^2 \rangle_v$ has the same oscillating amplitude on the ripples until it reaches the saturated value. The effect about acceleration is clear in the early time region if we compare the UAD detector curve with the inertial detector curve.

Figure 11 shows $\langle \dot{Q}(\eta)^2 \rangle$ for an inertial detector. Comparing with the Figure 6 (i.e. $\langle \dot{Q}(\eta)^2 \rangle$ for UAD), the curve for UAD is decreasing to a saturated value which is different from the inertial case. This feature can be seen from the term $\langle Q(\eta)^2 \rangle$, for example in Figure 3 the amplitude of the oscillations becomes small gradually and this implies that the changes of $\langle \dot{Q}(\eta)^2 \rangle$ also become small as τ increases. This is a clear feature for UAD that its magnitude of $\langle \dot{Q}(\eta)^2 \rangle$ is decreasing in the early time region.

So far, from Figure 3 to Figure 11 we can see that the difference between the inertial detector and UAD is clear in the plots for the two-point correlation functions $\langle Q(\eta)^2 \rangle$ and $\langle \dot{Q}(\eta)^2 \rangle$. For the two-point function $\langle Q(\eta)^2 \rangle$ of UAD, the curve has a larger oscillations at first and then shrinks to a smaller oscillations, and the magnitude does not change much from the beginning to the end. On the contrary, the amplitude of the oscillations for the two-point function $\langle Q(\eta)^2 \rangle$ for the inertial detector does not shrink in the beginning and the magnitude increases from the beginning until to the saturated region. For the two-point function $\langle \dot{Q}(\eta)^2 \rangle$, the difference between the UAD and inertial detector is more obvious that the curve for $\langle \dot{Q}(\eta)^2 \rangle$ of UAD is decreasing to a saturated value, while the curve for the inertial detector is increasing. The effect of the proper acceleration is shown in the two-point correlation functions $\langle Q(\eta)^2 \rangle$ and $\langle \dot{Q}(\eta)^2 \rangle$.

We think that the difference is from the Unruh effect that the uniformly accelerated detector would experience a thermal bath at temperature $T_U = \hbar a / (2\pi c k_B)$, where a is the proper acceleration. This thermal bath changes the two-point correlation functions.

IV. SUMMARY

We investigate the two moving detectors system Alice and Bob in a quantum field. In this system, Alice is static while Bob is either uniformly accelerating or moving at constant velocity. We apply two different types of trajectories for such set up and calculate the solutions for the internal degree of freedom Q for the moving detector Bob under the influence of the background quantum field. In this work, we find the following points:

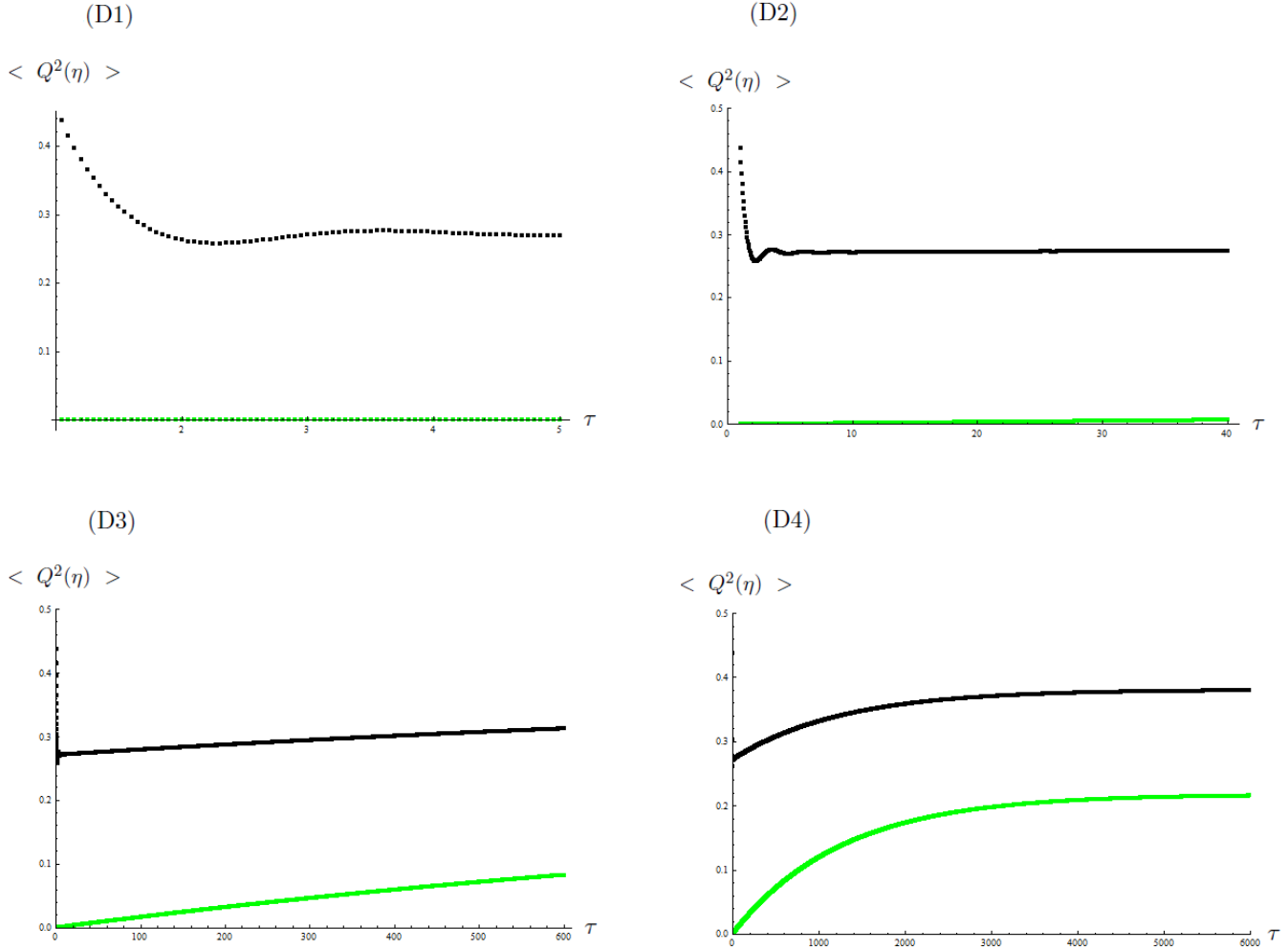


FIG. 10: The two point correlation function $\langle Q(\eta)^2 \rangle_v$ for an inertial detectors. Here $a = 0.001$, $\gamma = 0.000398$ ($\lambda_0 = 0.1$), $m_0 = \hbar = 1$ and $\Omega = 1$. Two different time scale are shown on these two plots. In the beginning, the value increases slowly with ripples on the curve and then reaches a saturated value at late time.

(1) The inertial worldline we need for the two moving detectors to exchange the signals within a reasonable finite time interval can not be replaced by the UAD trajectory in Rindler space $z_B^\mu = (a^{-1} \sinh a\tau, a^{-1} \cosh a\tau, 0, 0)$ by setting the proper acceleration $a = 0$. When the proper acceleration in the Rindler space goes to zero, the UAD worldline is shifted to very far away such that Alice and Bob no longer exchange signals in a reasonable time interval. Therefore, we need to apply a true trajectory $\tilde{z}_B^\mu = (\gamma\tau, \gamma v\tau + x_a + d, 0, 0)$ for a detector moves at constant velocity. By using this trajectory \tilde{z}_B^μ , Bob is away from Alice the distance "d" so that they can exchange the signal in a finite time interval. We can apply this trajectory to compute the two-point functions $\langle Q(\eta)^2 \rangle$ and $\langle \dot{Q}(\eta)^2 \rangle$ for the inertial detector, and compare the two-point correlation functions $\langle Q(\eta)^2 \rangle$ and $\langle \dot{Q}(\eta)^2 \rangle$ for the UAD and inertial detector.

(2) We find that a term is missing in both two-point correlation functions $\langle Q(\eta)^2 \rangle_v$ and $\langle \dot{Q}(\eta)^2 \rangle_v$ in the past calculations. Without this term, the variance from the quantum field part of the inertial detector is "0" (i.e. $\langle Q(\eta)^2 \rangle_v = 0$), which is highly unlikely. However, if the missing term is included, the variance from the quantum field for the inertial detector is nonzero and this is the property we expect for a moving detector interacts with a quantum field. The missing term also changes the behavior of the two-point correlation functions $\langle Q(\eta)^2 \rangle_v$ and $\langle \dot{Q}(\eta)^2 \rangle_v$ for UAD and this point is not noticed before.

(3) The values of the parameters in this model has an allowed region. We apply the perturbation method to obtain the solutions for Q , therefore the parameters in this model should obey the basic assumption of perturbations that

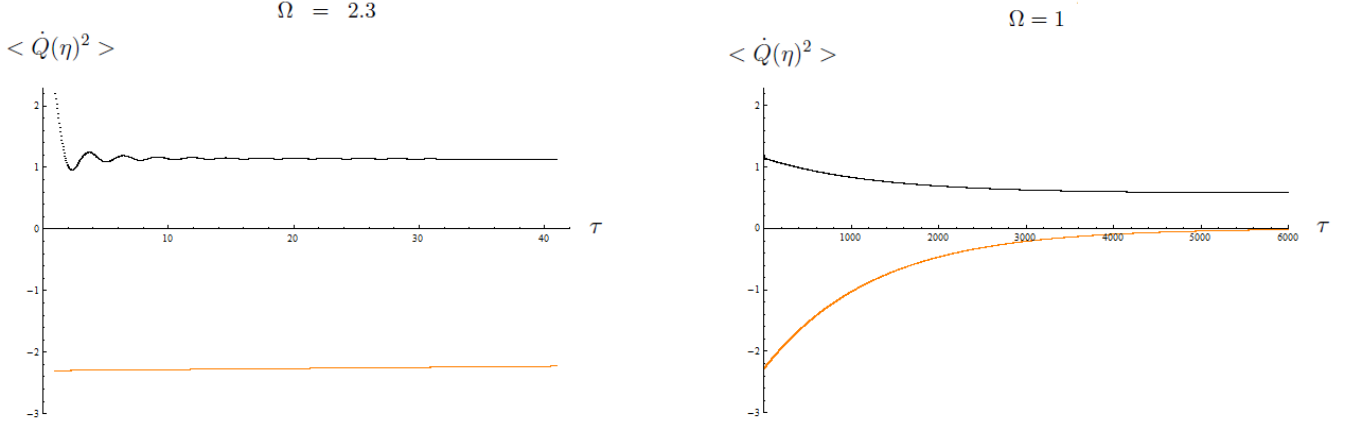


FIG. 11: The two point correlation function $\langle \dot{Q}(\eta)^2 \rangle$ for an inertial detectors. Here $a = 0.001$, $\gamma = 0.000398$ ($\lambda_0 = 0.1$), $m_0 = \hbar = 1$ and $\Omega = 1$. These plots are similar to the $\langle Q(\eta)^2 \rangle$ case. Two different time scale are shown in these two plots. In the beginning, the value of the two-point function increases slowly with ripples on the curve and then reaches a saturated value at later time.

next leading order must be smaller than the leading order. In the past work, we did not notice this part and took the decay parameter γ to be $\gamma = 0.1$, which means the expansion parameter λ_0 is larger than 1 (when $\gamma = 0.1$ the coupling constant $\lambda_0 \simeq 1.58$). This value of γ is inconsistent with the basic assumption of the perturbation and will give us some artefact. And, this will result in a misleading to the effect about the proper acceleration.

(4) Including above considerations, the UAD and inertial detector have different behavior on $\langle Q(\eta)^2 \rangle_v$ and $\langle \dot{Q}(\eta)^2 \rangle_v$. In early time region the two-point function $\langle Q(\eta)^2 \rangle_v$ for UAD has a quite flat curve while the inertial detector has an increasing curve. The amplitude of those oscillations on the ripples of the UAD curve gradually shrinks while the amplitude of the oscillations on the ripples of the inertial detector does not change. For the two-point function $\langle \dot{Q}(\eta)^2 \rangle_v$, the difference is more clear than $\langle Q(\eta)^2 \rangle_v$. The curve for $\langle \dot{Q}(\eta)^2 \rangle_v$ of the UAD is high at first and then decreases until it reaches to the saturated value. However, the curve of $\langle \dot{Q}(\eta)^2 \rangle_v$ for the inertial detector increases until it reaches to the saturated value. This part is quite different from the past result. We think that this implies that the proper acceleration a has some effects on the vacuum state of Q and thus affects the vacuum fluctuations of the UAD(Unruh effect).

The foundations of the calculations were built by Lin and Hu [21] by using the quantum field theory method and then it was applied to the two moving detectors system by Lin, Chou and Hu [23], these are not easy calculations. Here, base on their work, we redo the calculations and modify it. Since the calculation is tricky, we write down the detailed calculations for whom have interests about it.

In the future, we would like to apply this results to the quantum teleportation issue, for example two moving detectors system that Alice and Bob have relativistic motion to each other. We would like to see that whether the Unruh effect may play a role in the quantum teleportation process for two relatively moving detectors system.

V. ACKNOWLEDGEMENT

We would like to thank Dr. Shih-Yuin Lin, Dr. Chung-Hsien Chou, Dr. Jen-Tsung Hsiang and Dr. Ron-Chou Hsieh for helpful discussions, the encouragement and help from Professor Bei-Lok Hu and Professor Kin-Wang Ng. Special thanks for Dr. Shih-Yuin Lin for providing some detailed notes about the calculations of the two-point functions. This work is supported in part by the Ministry of Science and Technology, Taiwan under Grants No. MOST 106-2811-M-108-006 and Grants No. MOST 109-2112-M-001-003.

APPENDIX A: solving for $f_0^{(+)}, f^{(+)}, q^{(+)}, f^a$ and q^a

The method to obtain f and q are analogous to what we did in classical field theory [21]. Firstly, we find an expression relating the harmonic oscillator and the field amplitude right at the detector. Then substituting this relation into the equation of motion for the oscillator, we obtain a complete equation of motion for q with full information of the field. Then, we solve this complete equation of motion for q , and from its solution determine the field f consistently.

Eq.(18) implies that

$$(\partial_t^2 - \nabla^2)f^{(+)}(x; \mathbf{k}) = \lambda_0 \int_{\tau_0}^{\infty} d\tau \delta^4(x - z(\tau))q^{(+)}(\tau; \mathbf{k}). \quad (71)$$

The general solution for $f^{(+)}$ reads

$$f^{(+)}(x; \mathbf{k}) = f_0^{(+)}(x; \mathbf{k}) + f_1^{(+)}(x; \mathbf{k}), \quad (72)$$

where

$$f_0^{(+)}(x; \mathbf{k}) \equiv e^{-i\omega t + i\mathbf{k} \cdot \mathbf{x}} \quad (73)$$

is the free field solution, and

$$f_1^{(+)}(x; \mathbf{k}) \equiv \lambda_0 \int_{\tau_0}^{\infty} d\tau G_{\text{ret}}(x; z(\tau))q^{(+)}(\tau; \mathbf{k}) \quad (74)$$

is the retarded solution, which looks like the retarded field in classical field theory. Here $\omega = |\mathbf{k}|$ and the retarded Green's function G_{ret} in Minkowski space is given by

$$G_{\text{ret}}(x, x') = \frac{1}{4\pi} \delta(\sigma) \theta(t - t') \quad (75)$$

with $\sigma \equiv -(x_\mu - x'_\mu)(x^\mu - x'^\mu)/2$. Applying the explicit form of the retarded Green's function, one can go further to write

$$f_1^{(+)}(x; \mathbf{k}) = \frac{\lambda_0 \theta(\eta_-)}{2\pi a X} q^{(+)}(\tau_-; \mathbf{k}), \quad (76)$$

where

$$X \equiv \sqrt{(-UV + \rho^2 + a^{-2})^2 + 4a^{-2}UV}, \quad (77)$$

$$\tau_- \equiv -\frac{1}{a} \ln \frac{a}{2|V|} (X - UV + \rho^2 + a^{-2}), \quad (78)$$

$$\eta_- \equiv \tau_- - \tau_0, \quad (79)$$

with $\rho \equiv \sqrt{x_2^2 + x_3^2}$, $U \equiv t - x^1$ and $V \equiv t + x^1$.

The formal retarded solution (76) is singular on the trajectory of the detector. To deal with the singularity, note that the UD detector here is a quantum mechanical object, and the detector number would always be one. This means that at the energy threshold of detector creations, there is a natural cutoff on frequency, which sets an upper bound on the resolution to be explored in our theory. Thus it is justified to assume here that the detector has a finite extent $O(\Lambda^{-1})$, which will introduce the back reaction on the detector.

Let us regularize the retarded Green's function by invoking the essence of effective field theory:

$$G_{\text{ret}}^\Lambda(x, x') = \frac{1}{4\pi} \sqrt{\frac{8}{\pi}} \Lambda^2 e^{-2\Lambda^4 \sigma^2} \theta(t - t'). \quad (80)$$

(For more details on this regularization scheme, see Refs.[15, 25].) With this, right on the trajectory, the retarded solution for large Λ is

$$f_1^{(+)}(z(\tau); \mathbf{k}) = \frac{\lambda_0}{4\pi} [\Lambda \zeta q^{(+)}(\tau; \mathbf{k}) - \partial_\tau q^{(+)}(\tau; \mathbf{k}) + O(\Lambda^{-1})], \quad (81)$$

where $\zeta = 2^{7/4}\Gamma(5/4)/\sqrt{\pi}$. Substituting the above expansion into (17) and neglecting $O(\Lambda^{-1})$ terms, one obtains the equation of motion for $q^{(+)}$ with back reaction,

$$(\partial_\tau^2 + 2\gamma\partial_\tau + \Omega_r^2)q^{(+)}(\tau; \mathbf{k}) = \frac{\lambda_0}{m_0}f_0^{(+)}(z(\tau); \mathbf{k}). \quad (82)$$

Fortunately, there is no higher derivatives of q present in the above equation of motion. Now $q^{(+)}$ behaves like a damped harmonic oscillator driven by the vacuum fluctuations of the scalar field, with the damping constant

$$\gamma \equiv \frac{\lambda_0^2}{8\pi m_0}, \quad (83)$$

and the renormalized natural frequency

$$\Omega_r^2 \equiv \Omega_0^2 - \frac{\lambda_0^2\Lambda\zeta}{4\pi m_0}. \quad (84)$$

In (82), the solution for $q^{(+)}$ compatible with the initial conditions $q^{(+)}(\tau_0; \mathbf{k}) = \dot{q}^{(+)}(\tau_0; \mathbf{k}) = 0$ is

$$q^{(+)}(\tau; \mathbf{k}) = \frac{\lambda_0}{m_0} \sum_{j=+,-} \int_{\tau_0}^{\tau} d\tau' c_j e^{w_j(\tau-\tau')} f_0^{(+)}(z(\tau'); \mathbf{k}), \quad (85)$$

where $f_0^{(+)}$ has been given in (73), c_{\pm} and w_{\pm} are defined as

$$c_{\pm} = \pm \frac{1}{2i\Omega}, \quad w_{\pm} = -\gamma \pm i\Omega, \quad (86)$$

with

$$\Omega \equiv \sqrt{\Omega_r^2 - \gamma^2}. \quad (87)$$

Throughout this paper we consider only the under-damped case with $\gamma^2 < \Omega_r^2$, so Ω is always real.

Similarly, from (17), (18), (25) and (26), the equations of motion for f^a and q^a read

$$(\partial_t^2 - \nabla^2) f^a(x) = \lambda_0 \int d\tau \delta^4(x - z(\tau)) q^a(\tau), \quad (88)$$

$$(\partial_\tau^2 + \Omega_0^2)q^a(\tau) = \frac{\lambda_0}{m_0}f^a(z(\tau)). \quad (89)$$

The general solutions for f^a , similar to (72), is

$$f^a(x) = f_0^a(x) + \lambda_0 \int_{\tau_0}^{\infty} d\tau G_{\text{ret}}(x; z(\tau)) q^a(\tau_-) \quad (90)$$

However, according to the initial condition (33), one has $f_0^a = 0$, hence

$$f^a(x) = \frac{\lambda_0\theta(\eta_-)}{2\pi a X} q^a(\tau_-). \quad (91)$$

Again, the value of f^a is singular right at the position of the detector. Performing the same regularization as those for $q^{(+)}$, Eq.(89) becomes

$$(\partial_\tau^2 + 2\gamma\partial_\tau + \Omega_r^2) q^a(\tau) = 0, \quad (92)$$

which describes a damped harmonic oscillator free of driving force. The solution consistent with the initial condition $q^a(\tau_0) = 1$ and $\dot{q}^a(\tau_0) = -i\Omega_r$ reads

$$q^a(\tau) = \frac{1}{2}\theta(\eta)e^{-\gamma\eta} \left[\left(1 - \frac{\Omega_r + i\gamma}{\Omega}\right) e^{i\Omega\eta} + \left(1 + \frac{\Omega_r + i\gamma}{\Omega}\right) e^{-i\Omega\eta} \right]. \quad (93)$$

APPENDIX B: the integration of κ

$$\begin{aligned}
& \langle Q(\tau - \tau_0)Q(\tau'' - \tau_0'') \rangle_v \\
&= \frac{\lambda_0^2 \hbar}{2m_0^2(2\pi)^2} \left[\sum_{j,j'=\pm} C_j C_{j'}^* \int_{-\infty}^{\infty} \frac{\kappa d\kappa e^{-i\kappa(\tau_0 - \tau_0'')}(e^{w_j(\tau - \tau_0)} - e^{i\kappa(\tau_0 - \tau)})(e^{w_{j'}^*(\tau'' - \tau_0'')} - e^{i\kappa(\tau'' - \tau_0'')})}{(1 - e^{-2\pi\kappa/a})(w_j + i\kappa)(w_{j'}^* - i\kappa)} \right. \\
&\quad \left. - \sum_{j,j'=\pm} C_j C_{j'}^* \int_{-\infty}^0 \frac{\kappa d\kappa e^{-i\kappa(\tau_0 - \tau_0'')}(e^{w_j(\tau - \tau_0)} - e^{i\kappa(\tau_0 - \tau)})(e^{w_{j'}^*(\tau'' - \tau_0'')} - e^{i\kappa(\tau'' - \tau_0'')})}{(w_j + i\kappa)(w_{j'}^* - i\kappa)} \right] \\
&= \langle QQ \rangle_{v1} - \langle QQ \rangle_{v2}, \tag{94}
\end{aligned}$$

$$\begin{aligned}
& \langle QQ \rangle_{v1} \\
&= \frac{\lambda_0^2 \hbar}{2m_0^2(2\pi)^2} \sum_{j,j'=\pm} C_j C_{j'}^* \int_{-\infty}^{\infty} \frac{\kappa d\kappa e^{-i\kappa(\tau_0 - \tau_0'')}(e^{w_j(\tau - \tau_0)} - e^{i\kappa(\tau_0 - \tau)})(e^{w_{j'}^*(\tau'' - \tau_0'')} - e^{i\kappa(\tau'' - \tau_0'')})}{(1 - e^{-2\pi\kappa/a})(w_j + i\kappa)(w_{j'}^* - i\kappa)} \\
&= \frac{\lambda_0^2 \hbar}{2m_0^2(2\pi)^2} \sum_{j,j'=\pm} \frac{C_j C_{j'}^*}{w_j + w_{j'}^*} \int_{-\infty}^{\infty} \frac{d\kappa}{1 - e^{-2\pi\kappa/a}} \left(\frac{w_j}{\kappa - iw_j} + \frac{w_{j'}^*}{\kappa + iw_{j'}^*} \right) (e_1 + e_2 + e_3 + e_4) \\
&= P_1 + P_2 + P_3 + P_4, \tag{95}
\end{aligned}$$

$$e_1 = e^{-i\kappa(\tau_0 - \tau_0'') + w_j(\tau - \tau_0) + w_{j'}^*(\tau'' - \tau_0'')}, \tag{96}$$

$$e_2 = -e^{w_j(\tau - \tau_0) + i\kappa(\tau'' - \tau_0)}, \tag{97}$$

$$e_3 = -e^{w_{j'}^*(\tau'' - \tau_0'') - i\kappa(\tau - \tau_0'')}, \tag{98}$$

$$e_4 = e^{i\kappa(\tau'' - \tau)}. \tag{99}$$

where

$$\begin{aligned}
P_1 &= \frac{\lambda_0^2 \hbar}{2m_0^2(2\pi)^2} \sum_{j,j'=\pm} \frac{C_j C_{j'}^*}{w_j + w_{j'}^*} \int_{-\infty}^{\infty} \frac{d\kappa}{1 - e^{-2\pi\kappa/a}} \left(\frac{w_j}{\kappa - iw_j} + \frac{w_{j'}^*}{\kappa + iw_{j'}^*} \right) e^{-i\kappa(\tau_0 - \tau_0'') + w_j(\tau - \tau_0) + w_{j'}^*(\tau'' - \tau_0'')} \\
&= \frac{\lambda_0^2 \hbar}{2m_0^2(2\pi)^2} \sum_{j,j'=\pm} \frac{C_j C_{j'}^*}{w_j + w_{j'}^*} e^{w_j(\tau - \tau_0) + w_{j'}^*(\tau'' - \tau_0'')} \cdot (-2\pi i) \cdot \\
&\quad \left[\frac{a}{2\pi} \sum_{n=-\infty}^{-1} \left(\frac{w_j}{ina - iw_j} + \frac{w_{j'}^*}{ina + iw_{j'}^*} \right) e^{-na(\tau_0 - \tau_0'')} + \frac{w_j e^{w_j(\tau_0 - \tau_0'')}}{1 - e^{-2i\pi w_j^*/a}} \right] \\
&= \frac{\lambda_0^2 \hbar}{2m_0^2(2\pi)^2} \sum_{j,j'=\pm} \frac{C_j C_{j'}^*}{w_j + w_{j'}^*} e^{w_j(\tau - \tau_0) + w_{j'}^*(\tau'' - \tau_0'')} \cdot \\
&\quad \left[\frac{w_j e^{-a(\tau_0 - \tau_0'')}}{1 + w_j/a} F_{w_j}(e^{-a(\tau_0 - \tau_0'')}) + \frac{w_{j'}^* e^{-a(\tau_0 - \tau_0'')}}{1 - w_{j'}^*/a} F_{-w_{j'}^*}(e^{-a(\tau_0 - \tau_0'')}) - \frac{2\pi i w_j e^{w_j(\tau_0 - \tau_0'')}}{1 - e^{-2i\pi w_j/a}} \right]. \tag{100}
\end{aligned}$$

$$\begin{aligned}
P_2 &= \frac{-\lambda_0^2 \hbar}{2m_0^2 (2\pi)^2} \sum_{j,j'=\pm} \frac{C_j C_{j'}^*}{w_j + w_{j'}^*} \int_{-\infty}^{\infty} \frac{d\kappa}{1 - e^{-2\pi\kappa/a}} \left(\frac{w_j}{\kappa - iw_j} + \frac{w_{j'}^*}{\kappa + iw_{j'}^*} \right) e^{w_j(\tau - \tau_0) + i\kappa(\tau'' - \tau_0)} \\
&= \frac{-\lambda_0^2 \hbar}{2m_0^2 (2\pi)^2} \sum_{j,j'=\pm} \frac{C_j C_{j'}^*}{w_j + w_{j'}^*} e^{w_j(\tau - \tau_0)} \cdot (2\pi i) \cdot \\
&\quad \left[\frac{a}{2\pi} \sum_0^{\infty} \left(\frac{w_j}{ina - iw_j} + \frac{w_{j'}^*}{ina + iw_{j'}^*} \right) e^{-na(\tau' - \tau_0)} + \frac{w_{j'}^* e^{w_{j'}^*(\tau'' - \tau_0)}}{1 - e^{2i\pi w_{j'}^*/a}} \right] \\
&= \frac{-\lambda_0^2 \hbar}{2m_0^2 (2\pi)^2} \sum_{j,j'=\pm} \frac{C_j C_{j'}^*}{w_j + w_{j'}^*} e^{w_j(\tau - \tau_0)} \cdot \left[\frac{w_j e^{-a(\tau'' - \tau_0)}}{1 - w_j/a} F_{-w_j}(e^{-a(\tau'' - \tau_0)}) \right. \\
&\quad \left. + \frac{w_{j'}^* e^{-a(\tau'' - \tau_0)}}{1 + w_{j'}^*/a} F_{w_{j'}^*}(e^{-a(\tau'' - \tau_0)}) + \frac{2\pi i w_{j'}^* e^{w_{j'}^*(\tau'' - \tau_0)}}{1 - e^{2i\pi w_{j'}^*/a}} \right]. \tag{101}
\end{aligned}$$

Since $e_3 = e_2^*|_{\tau \leftrightarrow \tau', \tau_0 \leftrightarrow \tau'_0}$, we have $P_3 = P_2^*|_{\tau \leftrightarrow \tau', \tau_0 \leftrightarrow \tau'_0}$. And,

$$\begin{aligned}
P_4 &= \frac{\lambda_0^2 \hbar}{2m_0^2 (2\pi)^2} \sum_{j,j'=\pm} \frac{C_j C_{j'}^*}{w_j + w_{j'}^*} \cdot \left[\frac{w_j e^{-a(\tau_0 - \tau_0'')}}{1 + w_j/a} F_{w_j}(e^{-a(\tau_0 - \tau_0'')}) \right. \\
&\quad \left. + \frac{w_{j'}^* e^{-a(\tau_0 - \tau_0'')}}{1 - w_{j'}^*/a} F_{-w_{j'}^*}(e^{-a(\tau_0 - \tau_0'')}) - \frac{2\pi i w_{j'}^* e^{w_j(\tau_0 - \tau_0'')}}{1 - e^{-2i\pi w_j/a}} \right]. \tag{102}
\end{aligned}$$

and we have used the formula below to show our results,

$$\sum_{n=1}^{\infty} = \frac{e^{-nx}}{n+y} = \frac{e^{-x}}{1+y} {}_2F_1(1+y, 1, 2+y, e^{-x}) \equiv \frac{e^{-x}}{1+y} F_{ay}(e^{-x}). \tag{103}$$

Now, combining P_1, P_2, P_3 and P_4 , and defining $\eta \equiv \tau - \tau_0$, $\eta'' \equiv \tau'' - \tau_0''$, the two point function $\langle Q(\eta)Q(\eta'') \rangle_{v1}$ is

$$\langle Q(\eta), Q(\eta'') \rangle_{v1} \equiv \frac{1}{2} \langle Q(\eta)Q(\eta'') + Q(\eta'')Q(\eta) \rangle_{v1} = Re\{P_1 + P_2 + P_3 + P_4\} \tag{104}$$

$$\begin{aligned}
\langle Q(\eta)^2 \rangle_{v1} &\equiv \lim_{\eta'' \rightarrow \eta} \frac{1}{2} \langle \{Q(\eta), Q(\eta'')\} \rangle_{v1} = \lim_{\eta'' \rightarrow \eta} Re\{P_1 + P_2 + P_3 + P_4\} \\
&= \frac{\hbar\gamma}{\pi m_0 \Omega^2} \theta(\eta) Re\{(\Lambda_0 - \ln \frac{a}{\Omega}) e^{-2\gamma\eta} \sin^2 \Omega\eta \\
&\quad + \frac{a}{2} e^{-(\gamma+a)\eta} \left[\frac{F_{\gamma+i\Omega}(e^{-a\eta})}{\gamma + i\Omega + a} \left(\frac{-i\Omega}{\gamma} \right) e^{-i\Omega\eta} + \frac{F_{-\gamma-i\Omega}(e^{-a\eta})}{\gamma + i\Omega - a} \left(\left(1 + \frac{i\Omega}{\gamma} \right) e^{i\Omega\eta} - e^{-i\Omega\eta} \right) \right] \\
&\quad - \frac{1}{4} \left[\left(\frac{i\Omega}{\gamma} + e^{-2\gamma\eta} \left(\frac{i\Omega}{\gamma} + 1 - e^{-2i\Omega\eta} \right) \right) (\psi_{\gamma+i\Omega} + \psi_{-\gamma-i\Omega}) \right. \\
&\quad \left. - \left(\frac{-i\Omega}{\gamma} + e^{-2\gamma\eta} \left(\frac{i\Omega}{\gamma} + 1 - e^{-2i\Omega\eta} \right) \right) i\pi \coth \frac{\pi}{a} (\Omega - i\gamma) \right] \}. \tag{105}
\end{aligned}$$

Here $\psi_s \equiv \psi(1 + \frac{s}{a})$ and $\Lambda_0 \equiv -\gamma_E - \ln \Omega |\tau_0 - \tau'_0|$ as $\eta' \rightarrow \eta$.

$$\begin{aligned}
&-\langle QQ \rangle_{v2} \\
&= \frac{-\lambda_0^2 \hbar}{2m_0^2 (2\pi)^2} \sum_{j,j'=\pm} c_j c_{j'}^* \int_{-\infty}^0 \frac{\kappa d\kappa e^{-i\kappa(\tau_0 - \tau_0'')} (e^{w_j(\tau - \tau_0)} - e^{i\kappa(\tau_0 - \tau)})(e^{w_{j'}^*(\tau'' - \tau_0'')} - e^{i\kappa(\tau'' - \tau_0'')})}{(w_j + i\kappa)(w_{j'}^* - i\kappa)} \\
&= \frac{-\lambda_0^2 \hbar}{2m_0^2 (2\pi)^2} \sum_{j,j'=\pm} \frac{c_j c_{j'}^*}{w_j + w_{j'}^*} \int_{-\infty}^0 d\kappa \left(\frac{w_j}{\kappa - iw_j} + \frac{w_{j'}^*}{\kappa + iw_{j'}^*} \right) (e_1 + e_2 + e_3 + e_4) \\
&= -\tilde{P}_1 - \tilde{P}_2 - \tilde{P}_3 - \tilde{P}_4, \tag{106}
\end{aligned}$$

$$\begin{aligned}
\tilde{P}_1 &= \frac{\lambda_0^2 \hbar}{2m_0^2(2\pi)^2} \sum_{j,j'=\pm} \frac{c_j c_{j'}^*}{w_j + w_{j'}^*} \int_{-\infty}^0 d\kappa \left(\frac{w_j}{\kappa - iw_j} + \frac{w_{j'}^*}{\kappa + iw_{j'}^*} \right) e^{-i\kappa(\tau_0 - \tau_0'') + w_j(\tau - \tau_0) + w_{j'}^*(\tau'' - \tau_0'')} \\
&= \frac{\lambda_0^2 \hbar}{2m_0^2(2\pi)^2} \left[\left(\frac{c_+ c_+^*}{w_+ + w_+^*} w_+ e^{w_+(\tau - \tau_0'') + w_+^*(\tau'' - \tau_0'')} + \frac{c_+ c_-^*}{w_+ + w_-^*} w_+ e^{w_+(\tau - \tau_0'') + w_-^*(\tau'' - \tau_0'')} \right) \right. \\
&\quad \cdot (-i2\pi - \Gamma(0, w_+(\tau_0 - \tau_0'')) + \log(w_+) + \log(\tau_0 - \tau_0'') - \log(w_+(\tau_0 - \tau_0''))) \\
&\quad + \left(\frac{c_- c_+^*}{w_- + w_+^*} w_- e^{w_-(\tau - \tau_0'') + w_+^*(\tau'' - \tau_0'')} + \frac{c_- c_-^*}{w_- + w_-^*} w_- e^{w_-(\tau - \tau_0'') + w_-^*(\tau'' - \tau_0'')} \right) \\
&\quad \cdot (-\Gamma(0, w_-(\tau_0 - \tau_0'')) + \log(w_-) + \log(\tau_0 - \tau_0'') - \log(w_-(\tau_0 - \tau_0''))) \\
&\quad - \left(\frac{c_+ c_+^*}{w_+ + w_+^*} w_+^* e^{w_+(\tau - \tau_0) + w_+^*(\tau'' - \tau_0)} + \frac{c_- c_+^*}{w_- + w_+^*} w_+^* e^{w_-(\tau - \tau_0) + w_+^*(\tau'' - \tau_0)} \right) \\
&\quad \cdot (\Gamma(0, -w_+^*(\tau_0 - \tau_0'')) + \log(-1/w_+^*) - \log(\tau_0 - \tau_0'') + \log(-w_+^*(\tau_0 - \tau_0''))) \\
&\quad - \left(\frac{c_+ c_-^*}{w_+ + w_-^*} w_-^* e^{w_+(\tau - \tau_0) + w_-^*(\tau'' - \tau_0)} + \frac{c_- c_-^*}{w_- + w_-^*} w_-^* e^{w_-(\tau - \tau_0) + w_-^*(\tau'' - \tau_0)} \right) \\
&\quad \cdot (\Gamma(0, -w_-^*(\tau_0 - \tau_0'')) + \log(-1/w_-^*) - \log(\tau_0 - \tau_0'') + \log(-w_-^*(\tau_0 - \tau_0''))) \left. \right] . \tag{107}
\end{aligned}$$

$$\begin{aligned}
\tilde{P}_2 &= \frac{\lambda_0^2 \hbar}{2m_0^2(2\pi)^2} \sum_{j,j'=\pm} \frac{c_j c_{j'}^*}{w_j + w_{j'}^*} \int_{-\infty}^0 d\kappa \left(\frac{w_j}{\kappa - iw_j} + \frac{w_{j'}^*}{\kappa + iw_{j'}^*} \right) e_2 \\
&= \frac{-\lambda_0^2 \hbar}{2m_0^2(2\pi)^2} \left[- \left(\frac{c_+ c_+^*}{w_+ + w_+^*} + \frac{c_+ c_-^*}{w_+ + w_-^*} \right) w_+ e^{w_+(\tau - \tau'')} \right. \\
&\quad \cdot (\Gamma(0, -w_+(\tau'' - \tau_0)) + \log(-1/w_+) + \log(-w_+(\tau'' - \tau_0)) - \log(\tau'' - \tau_0)) \\
&\quad - \left(\frac{c_- c_+^*}{w_- + w_+^*} + \frac{c_- c_-^*}{w_- + w_-^*} \right) w_- e^{w_-(\tau - \tau'')} \\
&\quad \cdot (\Gamma(0, -w_-(\tau'' - \tau_0)) + \log(-1/w_-) + \log(-w_-(\tau'' - \tau_0)) - \log(\tau'' - \tau_0)) \\
&\quad + \left(\frac{c_+ c_+^*}{w_+ + w_+^*} w_+^* e^{w_+(\tau - \tau_0)} + \frac{c_- c_+^*}{w_- + w_+^*} w_+^* e^{w_-(\tau - \tau_0)} \right) e^{w_+^*(\tau'' - \tau_0)} \\
&\quad \cdot (2\pi i - \Gamma(0, w_+^*(\tau'' - \tau_0)) + \log(w_+^*) - \log(w_+^*(\tau'' - \tau_0)) + \log(\tau'' - \tau_0)) \\
&\quad - \left(\frac{c_+ c_-^*}{w_+ + w_-^*} w_-^* e^{w_+(\tau - \tau_0)} + \frac{c_- c_-^*}{w_- + w_-^*} w_-^* e^{w_-(\tau - \tau_0)} \right) e^{w_-^*(\tau'' - \tau_0)} \\
&\quad \cdot (\Gamma(0, w_-^*(\tau'' - \tau_0)) - \log(w_-^*) + \log(w_-^*(\tau'' - \tau_0)) - \log(\tau'' - \tau_0)) \left. \right] . \tag{108}
\end{aligned}$$

$$\begin{aligned}
\tilde{P}_3 &= \frac{\lambda_0^2 \hbar}{2m_0^2(2\pi)^2} \sum_{j,j'=\pm} \frac{c_j c_{j'}^*}{w_j + w_{j'}^*} \int_{-\infty}^0 d\kappa \left(\frac{w_j}{\kappa - iw_j} + \frac{w_{j'}^*}{\kappa + iw_{j'}^*} \right) e_3 \\
&= \frac{-\lambda_0^2 \hbar}{2m_0^2(2\pi)^2} \left[-e^{w_+(\tau - \tau_0'')} \left(\frac{c_+ c_+^*}{w_+ + w_+^*} w_+ e^{w_+^*(\tau'' - \tau_0'')} + \frac{c_+ c_-^*}{w_+ + w_-^*} w_+ e^{w_-^*(\tau'' - \tau_0'')} \right) \right. \\
&\quad \cdot (-2\pi i + \Gamma(0, w_+(\tau - \tau_0'')) - \log(w_+) - \log(\tau - \tau_0'') + \log(w_+(\tau - \tau_0''))) \\
&\quad - e^{w_-(\tau - \tau_0'')} \left(\frac{c_- c_+^*}{w_- + w_+^*} w_- e^{w_+^*(\tau'' - \tau_0'')} + \frac{c_- c_-^*}{w_- + w_-^*} w_- e^{w_-^*(\tau'' - \tau_0'')} \right) \\
&\quad \cdot (\Gamma(0, w_-(\tau - \tau_0'')) - \log(w_-) - \log(\tau - \tau_0'') + \log(w_-(\tau - \tau_0''))) \\
&\quad - \left(\frac{c_+ c_+^*}{w_+ + w_+^*} w_+^* e^{w_+(\tau'' - \tau)} + \frac{c_- c_+^*}{w_- + w_+^*} w_+^* e^{w_+(\tau'' - \tau)} \right) \\
&\quad \cdot (\Gamma(0, -w_+^*(\tau - \tau_0'')) + \log(-1/w_+^*) - \log(\tau - \tau_0'') + \log(-w_+^*(\tau - \tau_0''))) \\
&\quad - \left(\frac{c_+ c_-^*}{w_+ + w_-^*} w_-^* e^{w_-^*(\tau'' - \tau)} + \frac{c_- c_-^*}{w_- + w_-^*} w_-^* e^{w_-^*(\tau'' - \tau)} \right) \left. \right]
\end{aligned}$$

$$\cdot (\Gamma(0, -w_-(\tau - \tau_0'')) + \log(-1/w_-^*) - \log(\tau - \tau_0'') + \log(-w_-(\tau - \tau_0''))) \] . \quad (109)$$

$$\begin{aligned} \tilde{P}_4 &= \frac{\lambda_0^2 \hbar}{2m_0^2(2\pi)^2} \sum_{j,j'=\pm} \frac{c_j c_{j'}^*}{w_j + w_{j'}^*} \int_{-\infty}^0 d\kappa \left(\frac{w_j}{\kappa - iw_j} + \frac{w_{j'}^*}{\kappa + iw_{j'}^*} \right) e_4 \\ &= \frac{\lambda_0^2 \hbar}{2m_0^2(2\pi)^2} \left[- \left(\frac{c_+ c_+^*}{w_+ + w_+^*} + \frac{c_- c_-^*}{w_- + w_-^*} \right) w_+ e^{-w_+(\tau'' - \tau)} \right. \\ &\quad \cdot (\Gamma(0, -w_+(\tau'' - \tau)) + \log(-1/w_+) - \log(\tau'' - \tau) + \log(-w_+(\tau'' - \tau))) \\ &\quad - \left(\frac{c_- c_+^*}{w_- + w_+^*} + \frac{c_- c_-^*}{w_- + w_-^*} \right) w_- e^{-w_-(\tau'' - \tau)} \\ &\quad \cdot (\Gamma(0, -w_-(\tau'' - \tau)) + \log(-1/w_-) - \log(\tau'' - \tau) + \log(-w_-(\tau'' - \tau))) \\ &\quad + \left(\frac{c_+ c_+^*}{w_+ + w_+^*} + \frac{c_- c_+^*}{w_- + w_+^*} \right) w_+^* e^{w_+^*(\tau'' - \tau)} \\ &\quad \cdot (2\pi i - \Gamma(0, w_+^*(\tau'' - \tau)) + \log(w_+^*) + \log(\tau'' - \tau) - \log(w_+^*(\tau'' - \tau))) \\ &\quad - \left(\frac{c_+ c_-^*}{w_+ + w_-^*} + \frac{c_- c_-^*}{w_- + w_-^*} \right) w_-^* e^{w_-^*(\tau'' - \tau)} \\ &\quad \cdot (\Gamma(0, w_-^*(\tau'' - \tau)) - \log(w_-^*) - \log(\tau'' - \tau) + \log(w_-^*(\tau'' - \tau))) \] . \quad (110) \end{aligned}$$

As $\eta \rightarrow \eta''$ (that is $\tau'' \rightarrow \tau$ and $\tau_0'' \rightarrow \tau_0$)

$$\begin{aligned} -\langle Q^2(\eta) \rangle_{v2} &= -\lim_{\eta'' \rightarrow \eta} \langle \{Q(\eta), Q(\eta'')\} \rangle_{v2} = -\lim_{\eta'' \rightarrow \eta} \text{Re}\{\tilde{P}_1 + \tilde{P}_2 + \tilde{P}_3 + \tilde{P}_4\} \\ &= \frac{\lambda_0^2 \hbar}{2m_0^2(2\pi)^2} \theta(\eta) \text{Re}\{\Lambda_{0_{v2}} - \left(\frac{\gamma - i\Omega}{8\Omega^2\gamma} e^{-2\gamma(\tau - \tau_0)} - \frac{1}{8\Omega^2} e^{-2\gamma(\tau - \tau_0) + 2i\Omega(\tau - \tau_0)} \right) \right. \\ &\quad \cdot \left(-2i\pi + \log(-\gamma + i\Omega) - \log\left(\frac{1}{\gamma - i\Omega}\right) \right) - \left(\frac{\gamma + i\Omega}{8\Omega^2\gamma} e^{-2\gamma(\tau - \tau_0)} - \frac{1}{8\Omega^2} e^{-2\gamma(\tau - \tau_0) - 2i\Omega(\tau - \tau_0)} \right) \\ &\quad \cdot \left(\log(-\gamma - i\Omega) + \log\left(\frac{1}{\gamma + i\Omega}\right) \right) + \left(\frac{-\gamma + i\Omega}{8\Omega^2\gamma} + \frac{1}{8\Omega^2} \right) \cdot [\Gamma(0, (\gamma - i\Omega)(\tau - \tau_0)) \\ &\quad - \log(\gamma - i\Omega) - \log(\tau - \tau_0) + \log((\gamma - i\Omega)(\tau - \tau_0))] + \left(\frac{-\gamma - i\Omega}{8\Omega^2\gamma} + \frac{1}{8\Omega^2} \right) \\ &\quad \cdot [\Gamma(0, (\gamma + i\Omega)(\tau - \tau_0)) - \log(\gamma + i\Omega) - \log(\tau - \tau_0) + \log((\gamma + i\Omega)(\tau - \tau_0))] \\ &\quad + \left(\frac{\gamma + i\Omega}{8\Omega^2\gamma} e^{-2\gamma(\tau - \tau_0)} - \frac{1}{8\Omega^2} e^{-2(\gamma + i\Omega)(\tau - \tau_0)} \right) \cdot [2\pi i - \Gamma(0, (-\gamma - i\Omega)(\tau - \tau_0)) + \log(-\gamma - i\Omega) \\ &\quad + \log(\tau - \tau_0) - \log((- \gamma - i\Omega)(\tau - \tau_0))] + \left(\frac{-\gamma + i\Omega}{8\Omega^2\gamma} e^{-2\gamma(\tau - \tau_0)} + \frac{1}{8\Omega^2} e^{2(-\gamma + i\Omega)(\tau - \tau_0)} \right) \\ &\quad \cdot [\Gamma(0, (-\gamma + i\Omega)(\tau - \tau_0)) - \log(-\gamma + i\Omega) - \log(\tau - \tau_0) + \log((- \gamma + i\Omega)(\tau - \tau_0))] \\ &\quad + \left(\frac{-\gamma + i\Omega}{8\Omega^2\gamma} e^{-2\gamma(\tau - \tau_0)} + \frac{1}{8\Omega^2} e^{2(-\gamma + i\Omega)(\tau - \tau_0)} \right) \cdot [2\pi i + \Gamma(0, (-\gamma + i\Omega)(\tau - \tau_0)) - \log(-\gamma + i\Omega) \\ &\quad - \log(\tau - \tau_0) + \log((- \gamma + i\Omega)(\tau - \tau_0))] + \left(\frac{-\gamma - i\Omega}{8\Omega^2\gamma} e^{-2\gamma(\tau - \tau_0)} + \frac{1}{8\Omega^2} e^{-2(\gamma + i\Omega)(\tau - \tau_0)} \right) \\ &\quad \cdot [\Gamma(0, (-\gamma - i\Omega)(\tau - \tau_0)) - \log(-\gamma - i\Omega) - \log(\tau - \tau_0) + \log((- \gamma - i\Omega)(\tau - \tau_0))] \\ &\quad + \frac{i}{8\Omega\gamma} \cdot [-\Gamma(0, (\gamma + i\Omega)(\tau - \tau_0)) + \log(\gamma + i\Omega) + \log(\tau - \tau_0) - \log((\gamma + i\Omega)(\tau - \tau_0))] \\ &\quad + \Gamma(0, (\gamma - i\Omega)(\tau - \tau_0)) - \log(\gamma - i\Omega) - \log(\tau - \tau_0) + \log((\gamma - i\Omega)(\tau - \tau_0))] \\ &\quad + \left(\frac{1}{8\Omega^2} - \frac{(\gamma - i\Omega)}{8\Omega^2\gamma} \right) \cdot (-\log(\gamma - i\Omega) - \log(-\gamma - i\Omega)) + \left(\frac{1}{8\Omega^2} - \frac{(\gamma + i\Omega)}{8\Omega^2\gamma} \right) \\ &\quad \cdot (-2\log(\gamma + i\Omega) - 2\pi i) \} , \quad (111) \end{aligned}$$

where $\Lambda_{0_{v2}}$ contains those divergent parts $\Gamma(0, 0)$ and $\log(0)$ as $\tau'' \rightarrow \tau$ and $\tau_0'' \rightarrow \tau_0$ and are absorbed into the renormalized constant or coefficient in the experiment..

- [1] W. G. Unruh, Phys. Rev. **D14**, 870(1976).
- [2] P. G. Grove, Class. Quan. Grav. **3**, 801(1986).
- [3] D. J. Raine, D. W. Sciama and P.G. Grove, Proc. R. Soc. **A435**, 205(1991).
- [4] W. G. Unruh, Phys. Rev. **D46**, 3271(1992).
- [5] S. Massar, R. Parentani and R. Brout, Class. Quan. Grav. **10**, 385(1993)
- [6] S. Takagi, Proc. Theor. Phys. Suppl. **88**, 1(1986); V. L. Ginzburg and V. P. Frolov, Sov. Phys. Usp. **30**, 1073(1988).
- [7] F. Hinterleitner, Ann. Phys. **226**, 165(1993).
- [8] J. Audretsch and R. Müller, Phys. Rev. **D49**, 4056(1994); J. Audretsch, R. Müller and M. Holzmann, Phys. Lett. **199A**, 151(1995).
- [9] S. Massar and R. Parentani, Phys. Rev. **D54**, 7426, 7444(1996).
- [10] B. L. Hu and A. Raval, "Is there Radiation in the Unruh Effect?", arXiv:quant-ph/0012135.
- [11] A. Raval, Ph. D. Thesis, University of Maryland, College Park, 1996 (unpublished).
- [12] A. Raval, B. L. Hu and J. Anglin, Phys. Rev. **D53**, 7003(1996).
- [13] A. Raval, B. L. Hu and D. Koks, Phys. Rev. **D55**, 4795(1997).
- [14] S.-Y. Lin, Phys. Rev. **D68**, 104019(2003).
- [15] P.R. Johnson and B. L. Hu, Phys. Rev. D **65**, 065015 (2002).
- [16] E Schrödinger, Proc. Cambridge Philos. Soc. **31**, 555(1935).
- [17] E Schrödinger, Proc. Cambridge Philos. Soc. **32**, 446(1936).
- [18] A. Einstein, B. Podolsky and N. Rosen, Phys. Rev. **47**, 777(1935).
- [19] M. D. Reid, Phys. Rev. A **40**, 913(1989)
- [20] H. M. Wiseman, S. J. Jones and A.C. Doherty, Phys. Rev. Lett. **98**, 140402(2007); S. J. Jones, H. M. Wiseman and A.C. Doherty, Phys. Rev. A. **76**, 052116(2007)
- [21] S.-Y. Lin and B. L. Hu, Phys. Rev. D **73**, 124018 (2006).
- [22] Ioannis Kogias, Antony R. Lee, Sammy Ragy and Gerardo Adesso, PRL **114**, 060403 (2015).
- [23] S.-Y. Lin, Chung-Hsien Chou and B. L. Hu, Phys. Rev. D **78**, 125025 (2008).
- [24] S.-Y. Lin, Chung-Hsien Chou and B. L. Hu, Phys. Rev. D **91**, 084063 (2015).
- [25] C. R. Galley and B. L. Hu, Phys. Rev. **D72**, 084023 (2005); C. R. Galley, B. L. Hu and S.-Y. Lin, "Electromagnetic and gravitational self-force on a relativistic particle from quantum fields in curved space" [gr-qc/0603099].